Acoustic Horn Design, Numerical and Experimental Investigations of Ultrasonic Vibration Assisted Turning of Ti-6Al-4V

Rudranarayan Kandi

Department of Mechanical Engineering
National Institute of Technology Rourkela

Acoustic Horn Design, Numerical and Experimental Investigations of Ultrasonic Vibration Assisted Turning of Ti-6Al-4V

Dissertation submitted in partial fulfilment

of the requirements for the degree of

Master of Technology (by Research)

in

Mechanical Engineering

by

Rudranarayan Kandi

(Roll Number: 614ME1002)

based on research carried out

under the supervision of

Prof. Susanta Kumar Sahoo

Jan, 2017

Department of Mechanical Engineering
National Institute of Technology Rourkela

Department of Mechanical Engineering
National Institute of Technology Rourkela

Jan 05, 2017

Certificate of Examination

Roll Number: *614ME1002*

Name: *Rudranarayan Kandi*

Title of Dissertation: *Acoustic Horn Design, Numerical and Experimental Investigations of Ultrasonic Vibration Assisted Turning of Ti-6Al-4V*

We the below signed, after checking the dissertation mentioned above and the official record book (s) of the student, hereby state our approval of the dissertation submitted in partial fulfilment of the requirements for the degree of *Master of Technology by Research* in Mechanical *Engineering* at *National Institute of Technology Rourkela*. We are satisfied with the volume, quality, correctness, and originality of the work.

Prof. Susanta Kumar Sahoo Principal Supervisor	Prof. Santosh Kumar Sahoo Member, MSC
Prof. Mohammed Rajik Khan Member, MSC	Prof. Siba Sankar Mohapatra Chairperson, MSC
Head of the Department Prof. Siba Sankar Mohapatra	Dr. Joyjeet Ghose External Examiner

Department of Mechanical Engineering
National Institute of Technology Rourkela

Prof. Susanta Kumar Sahoo

Professor

Jan 05, 2017

Supervisor's Certificate

This is to certify that the work presented in the dissertation entitled *Acoustic Horn Design, Numerical and Experimental Investigations of Ultrasonic Vibration Assisted Turning of Ti-6Al-4V* submitted by *Rudranarayan Kandi*, Roll Number 614ME1002, is a record of original research carried out by him under our supervision and guidance in partial fulfilment of the requirements for the degree of *Master of Technology by Research* in *Mechanical Engineering*. Neither this dissertation nor any part of it has been submitted earlier for any degree or diploma to any institute or university in India or abroad.

_____

Prof. Susanta Kumar Sahoo
Professor

Dedication

Dedicated to my beloved parents, lovable friends, and respected teachers

Rudranarayan Kandi

Declaration of Originality

I, *Rudranarayan Kandi*, Roll Number *614ME1002* hereby declare that this dissertation entitled *Acoustic Horn Design, Numerical and Experimental Investigations of Ultrasonic Vibration Assisted Turning of Ti-6Al-4V* presents my original work carried out as an M. Tech. (by Research) student of NIT Rourkela and, to the best of my knowledge, contains no material previously published or written by another person, nor any material presented by me for the award of any degree or diploma of NIT Rourkela or any other institution. Any contribution made to this research by others, with whom I have worked at NIT Rourkela or elsewhere, is explicitly acknowledged in the dissertation. Works of other authors cited in this dissertation have been duly acknowledged under the sections "Reference" or "Bibliography". I have also submitted my original research records to the scrutiny committee for evaluation of my dissertation.

I am fully aware that in case of any non-compliance detected in future, the Senate of NIT Rourkela may withdraw the degree awarded to me on the basis of the present dissertation.

Jan 05, 2017

NIT Rourkela *Rudranarayan Kandi*

Acknowledgement

I, Rudranarayan Kandi, would like to express my special appreciation and thanks to my guide, ***Prof. Sushanta Kumar Sahoo***, Mechanical Engineering, National Institute of Technology, Rourkela for his continuous encouragement and priceless supervision during my research works. In the midst of the busy schedule, his sincere instructions and apt help has comprehended this research work in stipulated time.

I wish to express my deep sense of gratitude to ***Prof. Siba Sankar Mohapatra***, HOD, Mechanical Engineering, National Institute of Technology, Rourkela for giving me an opportunity to work on this project despite several departmental difficulties. I am very much obliged to have him as my Chairperson in Masters Scrutiny Committee (MSC). I am very much grateful to my MSC members: ***Prof. Prabal Kumar Ray,*** Department of Mechanical Engineering, **Prof. Mohammed Rajik Khan,** Department of Industrial Design, and **Prof. Santosh Kumar Sahoo**, Department of Metallurgical and Materials Engineering. I am thankful to all the faculty members and technical staffs of Department of Mechanical Engineering by allowing me laboratory facilities to carry out my research works. I acknowledge with special thanks to ***Mr. Arabinda Khuntia***, Production engineering laboratory, ***Mr. Somma Tigga***, Welding Shop, Mechanical Engineering.

I extend my special gratitude to ***Sushanta Sahu, Bikash Ranjan Moharana, Mantra Prasad Satpathy, Srikar Potnuru, V.B. Shaibu and Kasinath Das Mohapatra,*** who were my lab mates during my research works. I blissfully acknowledge to my seniors ***Sambit Kumar Mohapatra***, ***Swastik Pradhan***, ***Alok Ranjan Biswal***, and ***Subrat Kumar Bhuyan*** for their support during the stay in National Institute of Technology, Rourkela. I do my gratefulness to my beloved friends, ***Dilip Kumar Bagal***, ***Satyabrata Tripathy, Somen Biswal, Debasis Panda*** and ***Soubhagya Sahoo*** for their immense help and support in every aspect of my life. Finally, special thanks to my parents ***Mr. Khirod Kumar Kandi*** and ***Mrs. Kanaka Lata Das*** for all of the sacrifices that they have made on my behalf.

Jan 05, 2017
NIT Rourkela

Rudranarayan Kandi
614ME1002

Abstract

Titanium alloys have got wide ranges of applications in the field of aerospace, biomedical, and marine industries owing to its unique properties like high strength, exceptional corrosion resistance, and high strength to weight ratio. Still, characteristics like redduced thermal conductivity and high affinity towards the cutting tools limit the machinability of these alloys making these as the hard to cut alloys. Ultrasonic vibration assisted turning (UVAT) is one of the novel machining processes enhancing the machinability of titanium alloys compared to the conventional turning (CT). The process allows us to impose an ultrasonic vibration of 20 kHz with small amplitude of vibration on the cutting insert to get an intermittent cutting, unlike the conventional turning. The present work consists of three parts (i) design and analysis of acoustic horn along with its fabrication (ii) finite element model for both of the processes and experimental investigation with the discussions, and (iii) machinability investigations of both the processes studying chip morphology, surface integrity and tool wear. The first part includes designing and modeling of the horn that will act as the tool holder in UVAT process, using Ansys v15®, along with the fabrication of the parts based on the analysis. The tool holder is stepped type made of stainless steel (Grade SS304) with flexible attachments for the cutting inserts. The later part of the thesis includes preparation of 3D thermo-mechanical finite element model for both the processes using Deform 3D®. Experimental investigations of both the machining processes were carried out to study the machinability of titanium Grade 5, TI-6Al-4V. The dependence of results (cutting force, surface roughness, tool temperature, chip morphology etc.) on the input parameters were investigated and compared. UVAT showed significant reductions in cutting forces with improved surface finish of the workpiece. In the third section, machinability indices like chip morphology, surface integrity, and tool wear were observed. The results confirm the suitability and advantages of the UVAT process compared to the CT process to machine hard to cut metal Ti-6Al-4V.

Keywords- Ti-6Al-4V; Ultrasonic vibration assisted turning; Acoustic horn; machinability; Finite element model; Machinability indices

Contents

List of Figures

List of Tables

Nomenclature

Symbols

A(x)	Cross sectional area
Adj R^2	Adjusted R- square
a	Amplitude
a_1	Uncut chip thickness
a_2	Chip thickness
B	Damping matrix
b_0 and b_1	Constants
C	Velocity of sound in horn material
D	Diameter of workpiece
d	Depth of cut
dm	Mass of element
E	Modulus of elasticity
F	Force acting axially
F_n	Force normal to shear plane
F_s	Shear force
F_x	Axial cutting force
F_y	Radial cutting force
F_z	Tangential cutting force
f	Ultrasonic frequency
f_{cs}	Chip Segmentation frequency
h	Global heat transfer coefficient
h_c	Convection coefficient constant
h_{max}	Peak height
h_{min}	Valley height
K	Stiffness matrix
K_1 and K_2	Correction factors

L	Resonant length of horn
M	Mass matrix
m	Friction factor
N	Rpm of the workpiece
n	Order of modes
Pred R^2	Predicted R- square
P_c	Pitch of the saw tooth
q	Heat flux
R	Radius of curvature
R^2	R-Square
R_a	Average surface roughness
r	Nose radius
s	Feed rate (mm/rev)
T	Cutting tool temperature
T_m	Melting temperature
T_r	Room temperature
T_t	Tool surface temperature during machining
T_w	Workpiece temperature
u	Displacement at distance, x
V_c	Cutting velocity
V_t	Cutting tool tip velocity
y	Output responses of dependent variable
%	Percentage
μm	Micro meter
ζ	Chip reduction coefficient
η	Friction angle
λ	Wavelength of vibration
ξ_1 and ξ_2	Amplitudes
ρ	Density

σ_x	Stress
Φ_s	Saw tooth angle
ω	Angular velocity
$\ddot{U}$	Acceleration vector
$\dot{U}$	Velocity vector
U	Displacement vector
ε	Plain strain
$\dot{\varepsilon}$	Strain rate
τ	Friction force

Abbreviations

2D	Two-dimensional
3D	Three-dimensional
ANOVA	Analysis of variance
CT	Conventional turning
CVD	Chemically vapour deposited
DAQ	Data acquisition system
Dof	Degree of freedom
FEM	Finite element model
GUI	Graphical user interface
R.E.	Relative error
SEM	Scanning electron microscope
TCWR	Tool workpiece contact ratio
UVAT	Ultrasonic vibration assisted turning

Chapter 1

Introduction

Advancement of science and innovation, improvement of modern creations and requirement of finished products with quality components are increasing day by day. Additionally, the final products should have possessed extraordinary properties like high strength, hardness, and corrosion resistance. To meet these needs, there is a rapid evolution of new materials and alloys like non-ferrous alloys, brittle and hard materials, and ceramic structures. Machining of these hard materials produces challenges like high cutting force, low tool life with an average surface quality. Turning operation has been extensively used as a material removal process in each industry. Therefore, industries are continuously asking and implementing novel machining methods. The ultrasonic vibration assisted turning (UVAT), in particular, is one of the novel innovations. It has been observed that the vibration assisted turning enhances the machinability of these difficult to cut materials reducing the cutting force, enhancing the tool life with an improved machined surface. Additionally, ultrasonic vibration assisted machining has a broad range of application and importance in the field of automobile, electronic industry, aerospace, marine, and biomedical industries. The present research has been carried out investigating the machinability of titanium alloy, Ti-6Al-4V using UVAT.

1.1 Titanium Alloys

The machining of Titanium alloys has got an extensive attention from industries like aerospace, medical, and biomedical plants, etc. due to its unique properties like light weight, high strength, high corrosion resistance and high strength to weight ratio. The application details [1-6] of this alloy are given in Table 1.1.

Despite these advantages, there arise several difficulties during the machining process of titanium alloys due to its inherent properties like high strength at elevated temperature, affinity to react with the tool and reduced thermal conductivity. These challenges in machining process make the titanium alloy as intractable or “hard to cut” alloy.

Table 1.1 Applications of titanium alloys in industries

Industries	Applications
Aerospace	Aircraft, armor plating, turbines, Jet engines
Marine	Propeller shafts, riggings, heat exchangers, Compressor blades
Biomedical	Dental implants, orthopedic implants
Chemical	Process pipes, heat exchangers, drums
Computer	Substrate for hard drives
Nuclear plant	Condenser tubing, Waste treatment parts

Further, the machining process of these alloys is associated with the major challenges like high-temperature evolution during the cutting, high pressure at the tool tip; chatter generation due to low elasticity modulus and tool wear [3, 6, 7]. Titanium alloys are classified into several categories, such as α-alpha alloys, near α- alloys, $\alpha+\beta$ alloys, and β alloys based on the composition percentage and lattice structures [1, 6, 8].The present work is based on the machining investigation of $\alpha+\beta$ alloys; Ti-6Al-4V, which is one of the most common alloy used in aerospace industry [7]. Titanium alloy (Grade 5), Ti-6Al-4V possesses the chemical compositions of 6% Aluminum (Al), 4% Vanadium (V), 0.20% Oxygen (O), 0.015% Phosphorous (P), and 89.75% Titanium (Ti). The presence of aluminum increases the alpha transformation temperature and is called as the alpha stabilizers, further making the alloy low dense. The additive like Vanadium produces the decreases in the beta transformation temperature, called the beta stabilizer providing additional strength to the alloy [2, 7, 9].

1.2 Turning Operation

Turning operation is a basic and universal machining process in production engineering. It is a material removal process in which a cutting tool is mounted on a tool post cutting the rotating job fixed at the chuck of a lathe machine to get the desired shape as shown in Figure 1.1.

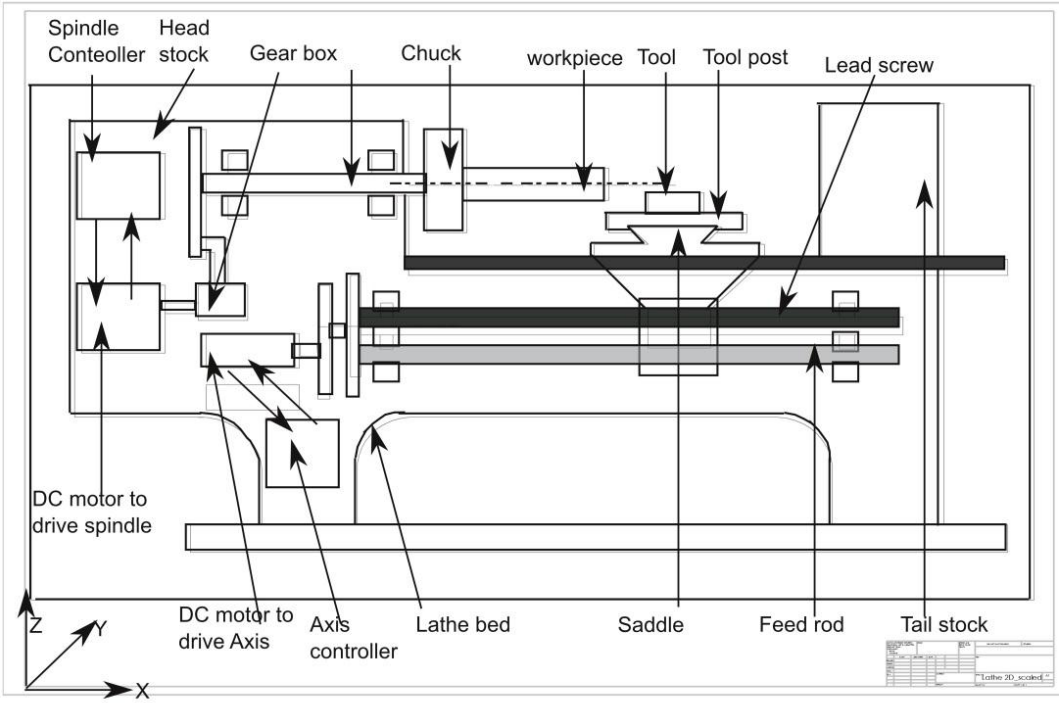

Figure 1.1 Line diagram for Lathe

Moreover, the introduction of metals and alloys with high hardness gradually required novel machining process mainly due to the high cost of hard cutting tools. So, several new machining processes were investigated and introduced to the turning process, such as hot turning, high-speed turning, turning with the cryogenically treated cutting tool, ultrasonic vibration assisted turning, thermally enhanced ultrasonic vibration assisted turning, laser assisted turning, and plasma assisted turning, etc. [10-18]. The present work is more focused to the ultrasonic vibration assisted turning.

1.2.1 Conventional turning (CT)

The conventional turning has been found to be very challenging work to process the intractable or "hard to cut" alloys. The inherent properties of Ti-6Al-4V like reduced thermal conductivity, work hardening, high hardness at elevated temperature and affinity to react with the workpiece limit its machining process. Therefore, there is a need for an alternative machining method to process these alloys and ultrasonic vibration assisted turning is one of the novel methods to process these alloys.

1.2.2 Cutting force

The primary response that affects the machinability of the certain job depends on the cutting force generation due to high pressure and friction during the process. It directly influences the tool life and power consumption controlling the production cost. In turning operation, the force components can be classified into three components like tangential cutting force (F_z), radial cutting force (F_y) and axial cutting force (F_x). F_z is also called as the principal or main cutting force along the direction of cutting velocity; F_x is the feed force along the feed direction and F_y is called radial force. Resultant force can be represented as follows,

$$R = F_z + F_{xy} \text{ and } F_{xy} = F_x + F_y$$

Further, the principal cutting force, F_z has the major role in power consumption whereas the machined surface accuracy and vibration are affected by the feed force, F_x. To model the cutting forces and correlating with the chip tool interface, cutting force model is explained with the help of Merchant's Circle (Figure 1.2). The different forces indicated in the merchant circles are described as follows,

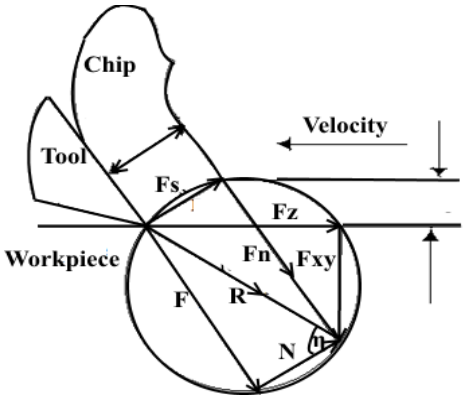

Figure 1.2 Merchant's Circle diagram [19]

Resultant force, R is the resultant of main cutting force, F_z and thrust force, F_{xy}. Also, the tool rake force, F and normal force, N results the resultant force, R. The ratio of F and N results the friction angle (η). Further, resultant can be formulated from the shear force, F_s along the shear plane and the force normal to the shear plane, F_n. The cutting forces mainly F_z, F_y and F_x can be measured using dynamometer mounted on the tool post of the lathe machine.

1.2.3 Cutting temperature

Temperature evolution during turning operation is due to the friction between the tool and workpiece or chip surface, has a direct effect on the tool wear. Therefore, temperature measurement or prediction of interface temperature has always been a challenging task for the researchers. As far as thermal effects are concerned, cutting temperature distribution is a most desired factor which needs to be accurately predicted to analyze wear rate, tool life, thermal stress and tool chipping in order to identify the optimum cutting conditions, tool design, and coating to improve the cutting capability. Some researchers investigated the cutting temperature during conventional turning using the photographic technique, embedded thermocouples, high speed thermal video camera and a high resolution thermographic system and also using some innovative methods like the inverse procedure for heat flux [20-22]. The major heat sources (Figure. 1.3) during turning operation are,

(a) The shear zone where the main plastic deformation occurs. It has the maximum contribution to the temperature evolution.
(b) Chip tool interface zone, where deformation occurs between the heated chip and the rake face of the tool
(c) The work-tool interface due to rubbing action between the flank face and the work.

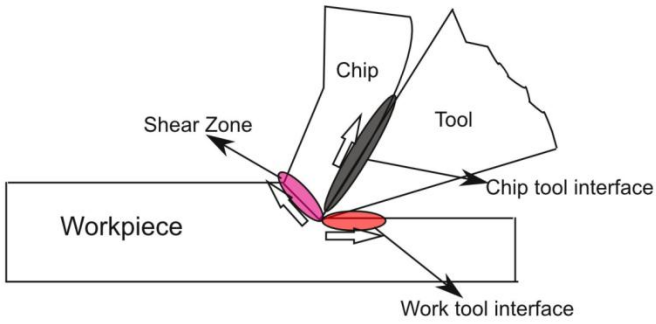

Figure 1.3 Heat sources in metal cutting [19]

1.2.4 Chip formation

The material removal process during turning process occurs in the form of chips. The nature of chip is a primary index that explains,

(a) Nature and characteristics of workpiece material
(b) Interaction at the chip tool interface

(c) Specific energy

The chip can be categorized into several types such as continuous chip, discontinuous chip and segmented chip as shown in Figure 1.4. The continuous chips are mostly formed during the turning of ductile material with a combination of high speed and low feed. Discontinuous chips are observed during machining of brittle jobs. Despite these, larger feed value with negative rake angle produces discontinuous chips. The segmented chip is produced during the machining of semi ductile and brittle jobs with a larger depth of cut with a cutting speed between low to medium.

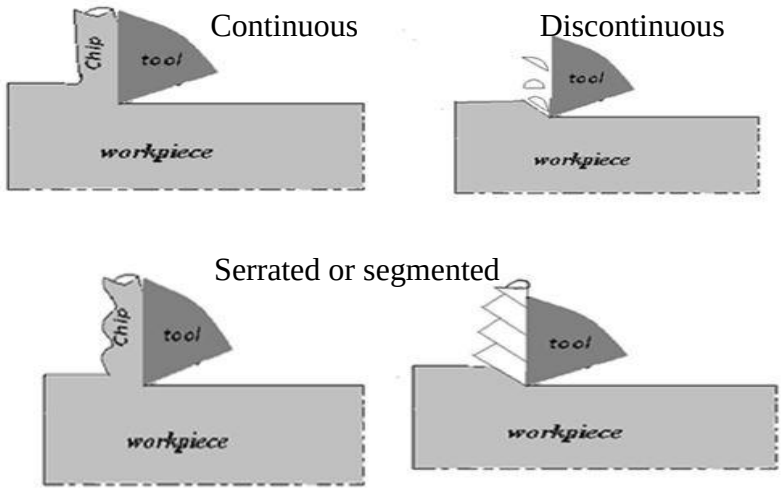

Figure 1.4 Various chips formed during turning process [19]

The formed chip geometry directly depends on,

a) Nature of workpiece material like ductile and brittle
b) Cutting insert geometry like rake angle, chip breaker
c) Cutting velocity and feed like low, medium and high speed
d) Cutting type like dry and wet cutting
e) Cutting temperature evolution etc.

To define the degree of plastic deformation, the chip geometry is expressed as chip reduction coefficient or cutting ratio. It is defined as the ratio of chip thickness to the uncut chip thickness. Since the chip thickness is larger due to compression of chip volume during machining compared to the uncut chip; the value is always greater than one. It can be expressed as,

$$\text{chip reduction coefficient}\,(\zeta) = \frac{a_2}{a_1} \quad (a_2 > a_1)$$

Where, ζ is the chip reduction coefficient, a_2 is the chip thickness and a_1 is the uncut chip thickness. Further, cutting controlling parameters like tool rake angle and wet turning affect the chip reduction coefficient.

1.2.5 Surface integrity

Surface integrity includes all the characteristics explaining the machined surface and can be classified as surface topography and surface metallurgy. Surface topography deals with the machined surface characteristics like surface texture and roughness, whereas, the second deals with the study of metallurgical and microscopic analysis of machined surface to differentiate the changed layer from the raw or base surface [19]. Different aberrations on the machined surface are surface defects, cracks, hardness alterations, residual stress, white layer formation and heat affected zone [19]. Surface integrity is one of the qualities to define the machinability of a job. Further, surface condition plays a critical role when applied under fatigue load conditions. Therefore, lots of researches have been carried out to study the surface integrity of titanium alloys [23-32].

1.2.6 Tool wear

Tool wear is one of the basic machinability indices that directly affect the machined surface controlling production economy. For a smooth machining process, the premature tool failure should be prevented. Tool failure generally happen due to several reasons, such as, mechanical breakage due to excessive load, high temperature evolution at the cutting zone and high strength of workpiece [19]. The tool wear can be broadly classified as mechanical wear and thermo-mechanical wear, chemical, and galvanic wear. The first includes wears like abrasion, chipping, deformation, adhesion, fracture, and flanking. The later includes wear due to diffusion and atomic migration. Chemical wear causes grooves on the tool surface due to chemical reactions at elevated temperature. Galvanic wear happens very rarely based on electrochemical dissolution. Different types of tool wear have been shown in Figure 1.5.

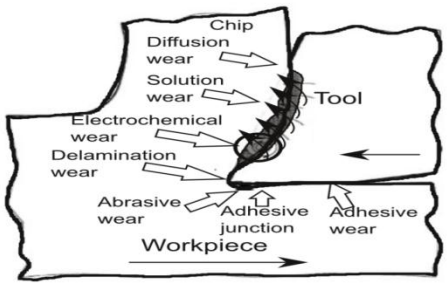

Figure 1.5 Tool wear region [33]

1.2.7 Ultrasonic vibration assisted turning (UVAT)

Ultrasonic vibration assisted turning is an innovative method to process the hard to cut alloys in which the cutting insert is subjected to a very high-frequency vibration, 20 kHz with a small amplitude. It has several advantages over conventional turning such as reduction in cutting forces with an improved machined surface and enhancing the tool life [18]. Ultrasonic vibration machining process was first introduced during the 1960s in which the vibration was applied onto the cutting tool with the help of a hydraulic vibrator with a vibration frequency range of 0-125 Hz [34]. Considering the turning operation and direction of vibration, it can be categorized into three parts as shown in Figure 1.6.

- UVAT with cutting insert vibrating in tangential direction
- UVAT with cutting insert vibrating in radial or depth of cut direction
- UVAT with cutting insert vibrating in axial or feed direction

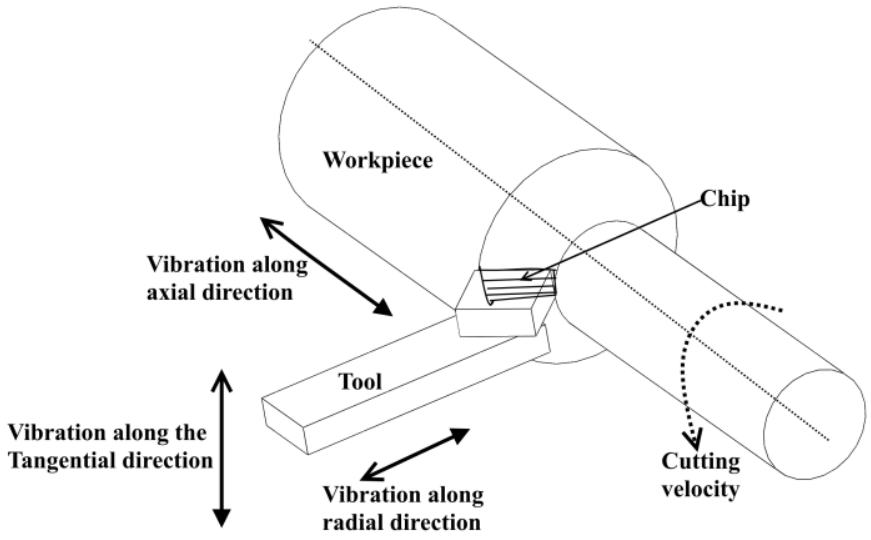

Figure 1.6 Different types of cutting vibrations in UVAT

1.2.8 Generation of ultrasonic vibration

The frequency range of the ultrasonic vibration starts from 20 kHz up to several gigahertzes that are not audible to human ear. Initially, the ultrasonic vibration was generated using magnetostrictive effect or joule's effect explained by Joule in 1842. Later, generation of the ultrasonic vibration with the piezoelectric effect was discovered by Jacques and Pierre Curie in 1880. The first application of this vibration was used to locate the submarines in the sea by Paul Langevin in 1917. At present, the ultrasonic vibration is generated mostly using piezoelectric effect due to less energy loss during the conversion of electrical energy to mechanical vibration. The piezoelectric transducer with ceramic plates is supplied with an electrical energy of 20 kHz frequency so that mechanical vibration with very small amplitude (~ 10μm) is generated due to the piezoelectric effect. To enhance the amplitude, concentrators or acoustic horns are linked between the transducer and the cutting tool. The ultrasonic vibration system consists of an ultrasonic generator, piezoelectric transducer, booster, and acoustic horn. Horns are different types such as cylindrical, conical, stepped, Bezier type, exponential and rectangular type [35, 36]. The horn acts as a tool holder in UVAT process and helps amplify the amplitude coming from the transducer and booster.

1.3 Need for Simulation Modelling

The direct investigation of a novel method using experimental work is always time-consuming and costly. Practically, in new and improved machining operation, there are complex responses such as process stability, material behavior, physical and thermal characteristics of the material which cannot be examined through repetitive experimental investigations from the economic point of view. Therefore, numerical methods with predictive models have been developed to improve the productivity enhancing the product quality. Finite element modeling is one the most used numerical method used by the researchers to predict, analyze, and solve the physical problems. In turning operations, the complex parameters like residual stress prediction, heat transfer among the contact parts, chip morphology, and process occurring at primary cutting zone have been predicted by several researchers using finite element model. There are several numerical models such as 2D and 3D model, thermo-mechanical model, thermo-viscoelastic model, visco-plastic

model, thermo-elastic plastic model, rigid-plastic model, Eulerian model, and ALE (Arbitrary Lagrangian Eulerian) model, etc. [37].

1.4 Motivation for the Present Research

There has been a growing demand in industries for new alloys with outstanding characteristics like light weight with high strength, corrosion resistance, and superior elasticity. Titanium alloy, Ti-6Al-4V is one of the alloys that extensively used in aerospace industries, marine, biomedical and oil industries. Still, due to properties like reduced thermal conductivity and high hardness at elevated temperature, the machining of this alloy has been a promising and challenging task using conventional methods. Ultrasonic vibration assisted turning is one of the novel machining process enhancing the machinability of these hard to cut alloy significantly reducing cutting forces with an improved machined surface and enhancing the tool life. Therefore, it is essential to investigate the machinability of these alloys during the ultrasonic vibration assisted turning. Unlike conventional turning models for this alloy, there are very few numerical models developed for the present process using this alloy.

Ample studies were made to find an optimum geometry of the concentrators or horns since the advantages of an ultrasonic vibration assisted turning are more prominent at a higher amplitude. Inversely, there is a heating problem as the amplitude increases. Past research says horns like stepped type and Bezier type have higher amplification compared to the other types. Therefore, it is essential to find out an innovative and flexible acoustic horn with higher amplification factor having flexible attachments for the economic point of view.

1.5 Aim and Objectives of the Present Work

The primary aim of the present research is to investigate the machinability of hard to cut titanium alloy, Ti-6Al-4V using ultrasonic vibration assisted turning. To fulfill the above target, the objectives are as follows:

1. Design and modeling of a flexible acoustic horn for the ultrasonic vibration assisted turning with finite element method (Performing modal and harmonic analysis) using an available academic package of Ansys v 15®.

2. Fabrication of the same based on the results obtained from the numerical analysis.
3. 3D finite element modeling of ultrasonic assisted turning for Ti-6Al-4V investigating process parameters and predicting various output responses like the transient behavior of stress, effective strain, interface temperature etc.
4. Experimental investigation of ultrasonic vibration assisted turning to study various effects of process parameters on the output responses.
5. Comparison of output responses (Cutting force, roughness, tool temperature etc.) obtained during ultrasonic vibration assisted turning with the conventional results
6. Model validation comparing the numerical results with the measured results
7. Investigation of machinability indices like chip morphology, surface integrity, tool wear.

1.6 Thesis Organization

There are seven chapters in the present work as follows,

Chapter 1- Introduction

It describes the application of hard to cut alloys like Ti-6Al-4V within various industries along with its properties. It covers a brief summary of conventional turning process and the need of novel technique, ultrasonic vibration assisted turning to process these alloys. Further, it explains few machinability indices along with various terminology related to turning operation.

Chapter 2- Literature review

It provides in-depth surveys related to turning process of titanium alloys, conventional turning, and ultrasonic vibration assisted turning, finite element modeling, machinability indices like chip morphology, surface integrity and tool wear. Moreover, this chapter helps to provide information emphasizing the need of present work.

Chapter 3- Design, modeling, and fabrication of acoustic horn

It explains different types of acoustic horns used for ultrasonic assisted manufacturing process. It includes design and modeling of a flexible acoustic horn for ultrasonic vibration assisted turning using finite element model.

Chapter 4- Experimental investigations

This chapter covers experimental design along with the experimental results for both the cutting operation. It explains the effects of cutting parameters on the output responses like force, tool temperature, and surface roughness. Further, it has a comparative analysis of machinability indices for both the cutting processes.

Chapter 5- Numerical Modelling and Comparison of Results

It explains modeling of the cutting processes using finite element model using commercial package, Deform 3D®. It covers the predicted results obtained from the simulation. Further, it includes the model validation comparing the results with the experimental results.

Chapter 6- Chip Morphology, Tool Wear, and Surface Integrity Investigations

It includes investigations of machinability indices like chip morphology, tool wear, and surface roughness. Chip morphology includes chip reduction coefficient, chip segmentation frequency. Tool wear includes both the flank and crater wears due to CT and UVAT.

Chapter 7- Conclusions

It contains major findings for the ultrasonic vibration assisted turning comparing with the conventional turning for both measured and numerical results. Also, it explains several works that needs to be done in the future to enhance the cutting process during ultrasonic vibration assisted turning. Finally, the work is enclosed with the list of references.

1.7 Closure

The present chapter discusses the importance of titanium alloys in different industries and their limitations during machining using conventional methods. The background of turning process with terminology related to it has been discussed. Moreover, the need of a novel machining process like ultrasonic vibration assisted turning and its applications have been examined. This chapter also explains the motivation and objectives of the present investigation.

Chapter 2

Literature Review

The motivation behind the literature review is to give foundation data on the issues to be considered in the present work and underscore the significance of the present study. The literature review extensively discusses the research works on the machining of titanium alloys, particularly Ti-6Al-4V with its demanding applications in various industries. The need of novel machining processes like ultrasonic vibration assisted turning to improve the machinability of this hard to cut alloys have been presented.

Turning operation is a standout amongst the most widely utilized material removal procedures, and its innovation keeps on progressing in parallel with the advancements in material science. The productivity and efficiency of a machining process depend on the cutting control parameters, environmental conditions, experimental apparatus, and workpiece and tool characteristics [38]. The ease with which a machining operation of material is carried out is called the machinability of that material. Prime machinability indices that affect the productivity and economy are surface roughness, cutting force, chip morphology, and tool wear [11, 39].

2.1 Turning of Titanium Alloys

Demand for new and special alloys in present industries has created advanced engineering materials and alloys with superior strength, outstanding corrosion and wear resistance with low weight to strength. Titanium alloys are used extensively in industries like aerospace, biomedical plants, turbocharger and turbine making plants [1, 4, 5, 9, 11, 39, 40]. But, properties like reduced thermal conductivity and high strength at an elevated temperature causing high tool temperature leading to fast tool wear rate and work hardening, make it an intractable or ‘hard to cut’ alloy [7, 9, 41-44]. The major challenges faced by researchers during the machining of these alloys are the short tool life with average surface finish due to the poor machinability. The reduced thermal conductivity and high hardness at elevated temperature result very high temperature evolution at the tool workpiece interface affecting the machinability in a negative way [44, 45].

The major problem in machining of titanium alloy is the tool wear due to high chemical reactive nature of the titanium towards the cutting tool resulting in the generation of build-up edges and high cutting force. Bhaumik et al. [41] investigated the turning operation of Ti-6Al-4V alloy using wBN-cBN composite tools. He suggested these cutting tools economically viable to process the hard to cut alloys. Machado et al. [2] studied different machinability indices like chip formation, tool wear and wear mechanism in turning of titanium and titanium alloys. Further, due to unavoidable challenges, the authors tried few novel machining processes like ultrasonic vibration assisted turning using rotary and ledge tools. Che-Haron et al. [46] studied the nature of both coated and uncoated cutting insert during the machining of titanium alloys. He concluded that the insert with finer grain size helped the machinability of these alloy enhancing the tool life with a better surface finish. Further, he noted that flank wear and excessive chipping at the flank wear were the prime cause of the tool wear. Ezugwu et al. [40] experimented using various cutting tools on the aerospace alloys for different cutting velocity ranges. He suggested for low speed cutting, cemented carbides (including coated carbides), ceramic tools and CBN tools could be the best suited insert to process the hard to cut alloys. For turning with high speed, CBN and ceramic tools can be the most economic insert for continuous machining of aerospace alloys. Further, researchers made special cutting tools to avoid the tool wear problem during the turning of Ti-6Al-4V [47]. Cemented carbide insert with 10% weight percentage of Ni_3Al was prepared with the help of spark plasma sintering method, and it showed significant resistance to flank and rake face wear.

Che- Haron et al. [26] carried out a dry turning operation of Ti-6Al-4V using uncoated carbide tool. The major findings were surface finish, microhardness of the machined surface and the metallographic study of the machined surface layer. He found that the surface roughness is significantly high due to the reduced thermal conductivity of the insert resulting severe tool wear. The machined surface was found with alteration of the microstructure along with a white layer of thickness 10 µm. Therefore, the machining of the intractable alloy was found to be a challenging task in the conventional machining. Ramesh et al. [31] analyzed the surface roughness obtained during the machining of Ti-6Al-4V with a multi-layered cutting insert and formulated it by means of ANOVA (Analysis of Variance). He found that the feed was the prime factor affecting surface roughness. Surface roughness increased to the maximum as the feed increased to a specific limit. The authors used a statistical method, response surface methodology (RSM)

to design the experiment and prepare a regression equation for the prediction purpose. Further, Chauhan et al. [48] examined the effect of cutting control parameters on the surface roughness while cutting Ti-6Al-4V with a polycrystalline diamond (PCD) with the RSM design. He observed that the feed, speed, and approach angle were the most influential factors affecting the surface roughness. As approach angle increases, there was an improvement in the machined surface. Ramesh et al. [49] studied the chip morphology and surface roughness while turning Ti-6Al-4V using a coated round insert, RCMT 10T300 using response surface methodology. Satyanarayana et al. [50] investigated the significance of back rake angle on the cutting force and surface roughness using Taguchi grey method during the turning of Ti-6Al-4V. Surface roughness characteristics depending on the various cutting control parameters like cutting velocity, feed and approach angle during turning of Ti-6Al-4V using coated insert were studied by Sharma et al. [51] and optimum parameters were identified. To achieve a sustainable turning operation of titanium alloy, Ti-6Al-4V, different types of lubricants such as cryogenic type, minimum quality lubrication (MQL), minimum quality cooled lubrication (MQCL) were used to reduce the friction coefficient [52]. Among these lubrications, MQL and MQCL with vegetable oils gave comparably acceptable results. Lin et al. [53] investigated the turning of Ti-6Al-4V using MQL to minimize the cost and pollution due to conventional cooling. Further, to increase the machinability of titanium alloy, Ti-6Al-4V in turning operation, researchers used lubricants with solid and suspended particles like graphite and molybdenum particles [54]. It was observed that cutting indices like tool wear, surface roughness, interface temperature and tool wear were marginally reduced on the application of lubricant with solid particles.

Venugopal et al. [12] studied the experimental investigation of Ti-6AL-4V using cryogenic liquid nitrogen as coolant. Since the high temperature evolution at the tool workpiece interface is the main reason for the wear propagation; the author used liquid nitrogen to increase the hardness of an ISO K20 grade cutting insert. Significant reductions in tool wear like adhesion, diffusion, and flank wear were observed at the end of the experiment. Moreover, Dhananchezian et al. [55] carried out turning of Ti-6Al-4V using a cryogenically cooled cutting insert and concluded that it significantly reduces the wear on the flank and rake surfaces along with the temperature reduction. Some researchers studied the machining of Ti-6Al-4V alloy obtained from the Electron beam melting technology (EBM) abundantly used in biomedical implants using coated insert

with dry and cryogenic lubricant [56]. The cryogenic cooling significantly reduced the adhesive wear reducing the machinability issues. Further, to enhance the machinability of Ti-6Al-4V, Nandy et al. [57] made an experimental set up with high pressure coolant jet that directly affected the cutting zone. He investigated several output responses like cutting force, chip morphology, tool life, and surface roughness. Unlike low pressure coolant, the high pressure coolant jet was more beneficial in reducing the cutting forces, improving the surface finish and tool wear. The similar type of experiment was carried out by Palanisamy et al. [58] during the turning of Ti-6Al-4V and found that the high pressure coolant enhanced the tool life with a better surface finish. Also, the application of high pressure coolant increased the chip serration frequency with higher strain rate. Additionally, to reduce the friction between the workpiece and tool for low temperature evolution, experiments were performed using micro- grooved cutting inserts [59]. Micro-grooved tool helps decrease the cutting force and temperature significantly. Additionally, Ma et al. [60] investigated the performance of micro-grooved tool while turning Ti-6Al-4V to reduce the cutting force and energy consumptions. Daymi et al. [61] studied the effect of cutting velocity on the chip morphology and force generation while cutting Ti-6Al-4V using a multi-layered coated insert. For different ranges of velocities, there were alternations in the chip geometries, such as continuous chip, flow chip, and segmented chips were obtained at 50 m/min, 100 m/min, and 150 m/min respectively. Moreover, the shear bands were more prominent during the high speed turning operation due to strain localization and high temperature generation. The force value was significantly reduced as the velocity increases from low to high cutting velocity. Cotterell et al. [62] formulated a thermal model numerically to understand the process occurring at the chip tool interface and rake face. Also, he examined the chip morphology and observed segmented chips for all possible runs varying the cutting velocity. The heat generation and tool temperature evolution on the rake face with the help of chip shape and chip color during turning of Ti-6Al-4V with dry and minimum quality lubrication (MQL) was experimented and predicted [63]. The chip formed during MQL was found to be more curled and white in color showing less heat generation. Dandekar et al. [44] investigated a hybrid machining process to improve the machinability of Ti-6AL-4V using coated tool. The experiment was a hybrid machining in which the hardness of the material was reduced using the laser impingement. He concluded that the hybrid machining process improved the machinability at the high range of cutting velocity enhancing the material removal rate, tool life, and surface finish. So, there has been a need for a new machining process to

increase the productivity while processing the titanium alloys. An et al. [64] studied on the turning of titanium alloy using cold water mist jet (CWMJ) instead of conventional lubrication to avoid the unwanted high temperature evolution during the turning operation. He concluded that the temperature and tool wear were drastically reduced during the use of CWMJ. Turning of titanium alloy, Ti-6Al-4V with ultra-hard cutting inserts like polycrystalline cubic boron nitride (PCBN) and polycrystalline diamond (PCD) were used to study the tool wear, temperature, surface roughness and microhardness.

2.2 Ultrasonic Vibration Assisted Turning (UVAT)

Due to rapid industrialization, there has been a growing demand for new and special material like super alloys and structural ceramics with unique properties like high strength, excellent corrosion resistance, and low weight to strength ratio. Therefore, researchers have been extensively exploring on new and novel machining methods to enhance the productivity along with the production economy. The ultrasonic vibration assisted turning (UVAT) is one of the novel machining method to process these intractable alloys in which very high frequency of 20 kHz with a small amplitude of 10 μm is imposed on the cutting tool with the help of an ultrasonic arrangement [65]. There is an extensive research in this field due to several advantages while machining using this method, such as reduction in cutting forces, enhancement of tool life, improved surface finish, and high material removal rate.

Initially, the vibration cutting was carried out by Kumabe [66] in which vibration was applied to the cutting tool to stabilize the cutting force characteristics during the turning operation. Further, the vibration assisted machining was studied by Kumabe and Hachisuka [67] observed an improved surface finish during the turning of plain carbon steels, stainless steel, and hardened steels. It has been reported that the material removal process was found to be marginally high while turning of ceramics [68]. The importance and advantages of vibration assisted turning were explained by Frederick [69]. The assessments revealed that the superposition of vibration onto the tool helped to reduce the cutting force with reduction in tool wear. Skelton et al. [34] allowed oscillation to the cutting tool in the tangential direction by means of a hydraulic vibrator during the turning process and marginally reduction in forces were observed. Zhou et al. [70] carried out turning of brittle material, fused silica applying ultrasonic vibration to a diamond cutting

tool. The reduction in cutting force and surface roughness was observed during low cutting velocity comparing with the conventional turning. Astashev [71] prepared a model for ultrasonic vibration assisted cutting with working frequency of 20 kHz and amplitude of 10 microns. He found significant reduction in cutting forces. He explained that the reduction in cutting forces depends on the cutting velocity and after a critical cutting velocity; there will be no advantages of vibration assisted turning. Additionally, a theoretical model along with the experimental investigation of the process superimposing vibration on the cutting tool was studied. Various dynamic characteristics like force reduction and material removal rate were studied along with a brief explanation of the stabilization of ultrasonic excitation. Kim et al. [72] investigated the machinability of highly demanding composite, CFRP (carbon fiber reinforced plastics) using ultrasonic vibration cutting (UVC). He observed that UVC helped the machinability with a cutting velocity within the range of critical velocity. Further, cutting velocity and feed were the most controllable parameters affecting the reduction of force and surface roughness.

For last decades, there were researches works carried out by several researchers on this novel machining process. A number of researchers have explained the mechanism behind UVAT. The main factor affecting the effective cutting in UVAT is the cutting tip velocity (V_t). Unlike conventional turning (CT), both of the workpiece and cutting inserts are in motion, one gets a rotational speed, and another gets a vibratory motion. The mechanism can be concluded with the expression (1) below [73, 74],

$$V_c = \frac{\prod DN}{1000} \langle V_t = \frac{120 \prod fa}{1000} \tag{1}$$

Where, Vc is Tangential cutting velocity due to spindle rotation (m/min), Vt is the maximum cutting velocity due to vibration (m/min), N is the rpm of the workpiece, D is the diameter of the workpiece (mm), f is the ultrasonic frequency, 20000 Hz and a is amplitude at the insert tip, (mm). The mechanism can be understood from the following Figure 2.1.

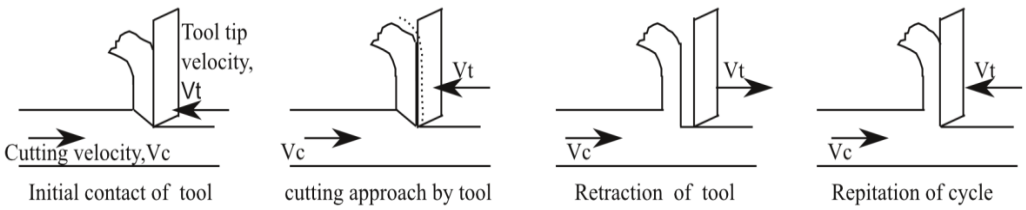

Figure 2.1 Cutting tool positions in UVAT [75]

Babitsky et al. [76] applied ultrasonic assisted turning on aviation materials like C263, Inconel 718 and mild steel with an ultrasonic vibration along the feed direction. The roughness and roundness of UVAT and CT machined workpiece were compared. The machined surface during vibration assisted turning was more improved than the conventional turning. Further, the chip formed during UVAT process was continuous without formation of built-up edges (BUE). To keep the vibration excitation stable during the turning operation, an innovative auto resonant set up was established. Further, experimental investigation and numerical simulations of both conventional turning and ultrasonic assisted turning were carried out to analyze the process occurring at the chip tool interface using MSC MARC® [73]. A numerical simulation model was validated with the experimental results explaining various stages of ultrasonic assisted turning, such as (a) approaching stage (b) penetration stage (c) unloading stage, and (d) withdrawal stage. Mitrofanov et al. [77] studied overall reductions in cutting forces, temperature distribution, residual stress and microhardness of surface layer . A thermo-mechanical model for ultrasonic assisted turning of Inconel 718 was prepared to investigate the tool temperature and interface temperature evaluation [78]. Also, the effect of heat transfer coefficient on the temperature evolution was discussed. Finite element model was developed for ultrasonic assisted turning using MSC MARC® to study the effect of cutting parameters like velocity, feed and depth of cut and lubrication type on the chip formation, forces, temperature distribution, and strain rate [79]. Plastic strain is found to be almost 15-20% high in case of ultrasonic assisted turning with a high material removal rate compared to the conventional turning. N Ahmed et al. [80] studied material responses like hardness, residual stress and change in microstructure during the machining of Inconel 718 . The average hardness of the surface using the ultrasonic assisted turning was 60% less than the conventional turning with a high value of residual stress. The simulation modelling using MSC-MARC® and analysis of ultrasonic vibration assisted turning of Inconel 718 were made by S. Amini [81]. He concluded that the cutting force depends on the cutting velocity and increases with increase in the latter. The effect of tool geometry on the UVAT process was quite similar to conventional turning. The increase in the amplitude of vibration resulted in significant reduction in cutting force during UVAT. Ahmed et al. [74] investigated the effect of turning and vibration parameters like cutting velocity, feed, amplitude, frequency, and direction of vibration on the cutting forces . He explained that the reduction of force with increase in amplitude and frequency was due to the increased cycle between the workpiece and tool during the intermittent motion of

cutting tool. Nath et al. [82, 83] carried out several experimental and theoretical investigations on ultrasonic vibration cutting of low alloys steel and Inconel 718. They claimed that to improve the quality of cutting, the tool workpiece contact ratio (TWCR) should be kept low. The major advantages of ultrasonic assisted turning were reduction in cutting forces, flank wear (12-25% reduction compared to CT) and improved surface quality. Further, they observed that at high cutting speed, there were catastrophic failures on the tool face due to impact loading of repeated vibrations. Also, the chip formed during UVAT was smooth, thin, and more curled than the chip formed during CT. Further, the authors studied on the elliptical vibration cutting to enhance the machinability of hard to cut alloys. The effect of cutting parameters like velocity, feed, depth of cut and nose radius on the output responses like force, surface roughness, and tool wear were investigated [84, 85].

Several researchers investigated the machinability of titanium alloys during ultrasonic vibration assisted turning. S. Koshimizu [86] assessed the ultrasonic vibration assisted turning (UVAT) of titanium alloy, Ti-6Al-4V and concluded that the UVAT was the most alternative process to reduce the force, tool wear, and surface roughness. The author mentioned that the UVAT is more effective when the cutting velocity is approximately 30% of the critical velocity. Muhammad et al. [87] studied the 3D finite element model for ultrasonic assisted oblique cutting of titanium alloy, Ti15V3Cr3Al3Sn. The research mainly adhered to the effect of cutting parameters like frequency, amplitude and contact conditions like with friction and without friction on the cutting forces only. Further, they carried out few hybrid machining processes like hot ultrasonically assisted turning or thermally enhanced ultrasonically assisted turning [15, 88-91]. They concluded that the material removal rate was comparatively high with an improved surface finish comparing with normal vibration assisted turning. Additionally, the authors prepared a thermo-mechanical model to predict the processes occurring at the chip tool interface, stress generation, and interface temperature. Patil et al. [92] assessed ultrasonic assisted turning of Ti-6Al-4V and concluded that cutting force increased due to increase in the cutting velocity. The machined surface obtained during UVAT was more improved compared to the CT machined surface. The metallographic study revealed that the microstructure of machined surface during UVAT was less deformed. Also, the chip produced during UVAT was more uniform, smooth, and thinner making this process superior than CT.

Nategh et al. [93] analyzed the hardness of lateral surface in oblique ultrasonic vibration assisted turning. He justified the effect of amplitude and cutting velocity on the ultrasonic assisted turning. UVAT will be more effective for higher amplitude and lower cutting velocity. A mechanistic friction model was prepared to study the effect of cutting speed and amplitude on the forces, tool-chip contact length, and friction coefficient and stress distribution for both CT and UVAT [94]. The model is a purely mathematical model, and the numerical results were compared with the measured results. Dong et al. [95] investigated UVAT of particle reinforced aluminum matrix. The major conclusions were based on the effect of tool geometry on the cutting forces, surface roughness, and tool wear. By applying ultrasonic vibration, cutting force and tool wear were significantly reduced compared to the CT process. The various types of tool wear found during the cutting processes were flank wear and wear due to abrasion and adhesion.

Khajehzadeh et al. [96] described the effects of different cutting parameters of UAT like feed rate, cutting velocity, amplitude, and frequency on temperature characteristics using embedded thermocouple experimentally. A mathematical model to analyze the mechanism of UVAT was prepared. They concluded that the UVAT is more effective when the cutting velocity is low with low feed rate. Further, he prepared and validated an FE model using ABAQUS® to investigate the cutting force and cutting temperature during both conventional and ultrasonic assisted turning using multicoated insert [75]. Cutting force magnitude was reduced by 10.86% when ultrasonic assisted turning was carried out with coated insert. Zou et al. [97] made a comparative study of CT and UVAT of austenitic stainless steel 304 (ASS). They concluded that with proper selection of cutting parameters like cutting velocity, feed, depth of cut including amplitude and frequency of vibration, UVAT can enhance the machinability of the demanding material austenitic stainless steel 304. There are several advantages due to the intermittent characteristics of the cutting tool during UVAT like reduction in cutting forces, high quality mirror surface is highly demanded in most of the industries and cannot be achieved by CT. However, Reduction in surface roughness generating mirror surface finished products has been observed during UVAT process [83]. UVAT shows a better cutting stability reducing the chattering unlike CT [98]. Low tool flank wear with long tool life, low wear and tear ratio and reduction in built up edges (BUE) formation have been noted during UVAT [82]. Further, the width of the generated hardened layer during CT has been found to 70%

higher that the layer generated during UVAT. It shows a quality machining during UVAT [80].

The intermittent motion of the tool during UVAT helps in reducing the cutting force. In UVAT, the rake face of the cutting insert repeatedly separated from the chip at the chip tool contact area with the ultrasonic frequency. It is also called cutting with ultrasonic vibration of the separate type.[99]. Due to this motion, the average contact time of the tool with the work piece decreases resulting in a force reduction. Further, the reduction in force is due to the reduction in friction between the tool and work piece due to the pulsating cutting tool [83]. This motion does not produce any built up edge (BUE) formation that leads to a high quality surface. Also, aerodynamic lubrication due to the vibration is another factor reducing the cutting force. During UVAT, it abolished BUE that reduces surface roughness. Since, during CT, the tool is in continuous engagement with the work piece, the feed marks and BUE formations are the fundamental reasons for the surface errors which are not prominent during UVAT [92]. The surface roughness during a turning process depends on the flank wear, BUE and chip formation. During CT, the contact is continuous type generating high temperature and friction that causes rapid wear to the tool and BUE formation. Due to pulsating characteristics of the tool during UVAT, the chips formed have been found to be sharper, thinner and smooth unlike the chips generated during CT. This also promises a better surface finish than the CT process [82].

Ultrasonic vibration assisted turning with the vibration along the cutting or tangential direction has been rigorously studied in the literature reviews. The advantages have been mentioned in the above modifications. Based on the survey, the experimental set up along with the ultrasonic system has been established. However, the vibration along the feed direction has been investigated by Babitsky [100] and observed that the application of vibration in feed direction has less limiting than the tangential direction. However, the effect will be more or less same for the UVAT process with the vibration along radial direction due to low magnitude of the amplitude.

2.3 Acoustic Horn

Ultrasonic vibration assisted turning (UVAT) is one of the noble machining processes. Unlike conventional turning (CT), a high frequency of 20 kHz with small amplitude, ≈10-15 μm is supplied to the tool using the acoustic system consisting of a transducer, booster,

and horn. The piezoelectric transducer converts the electrical source to the mechanical energy and transfers the energy through the booster which enhances the amplification of the frequency from the transducer. Finally, the vibration is supplied to the required surface for the machining process through the final horn with further amplification. In the present content, the process is ultrasonic vibration assisted turning (UVAT), and the horn or sonotrode acts as a tool holder for the insertion of cutting insert. Acoustic horns are also called the concentrator or sonotrode which is a major part of the ultrasonic system. There have been several researches on the acoustic horn design to make it stable during the vibration assisted turning process.

The horns are made of metals that have high fatigue strengths and low acoustic losses. Different types of horns like cylindrical, conical, exponential, and stepped and Bezier horns have been discussed by several researchers in the past [36, 101]. Since the advantages obtained from the UVAT over CT is due to the intermittent motion of the cutting insert attached to the horn, generally, the stepped and Bezier type horn possessing higher amplification compared to the other horns are used for this process [36]. Dynamic properties of different horns with different geometries were analyzed by M Nad [102]. Different dynamic characteristics of a horn, like natural frequency and amplification of the horn at the horn tip, slenderness ratio, and amplification ratio of various types of horns were analyzed. He found that the cause for reduction in amplification was due to the increase in slenderness ratio. Further, the dynamic properties of different shapes of the horn at different modes were studied. Seah et al. [35] carried out the modal analysis to find out the resonance frequency of acoustic horns like conical, exponential, and stepped types and determined the stress characteristics of the horns under operating conditions considering the dynamic characteristics. The parameters influencing the effective length of a stepped horn were discussed by Nanu et al. [103]. The principal factors which can be controlled for the tuning of the horn or natural frequency are the length of the horn, the radius of curvature, diameter, and making of the groove at the center of gravity of the horn, etc. The horn length and the radius of curvature at the nodal point were affecting the natural frequency, whereas, the amplification ratio was affected by diameter ratio. Theoretical and experimental results were compared and found to be in good agreement. Amin et al. [104] made both traditional and computation analysis using finite element method for different types of horns suggesting an optimized horn for the ultrasonic machining process. Amini et al. [81] examined various horn with cutting tools like

cylindrical horn with eccentric holder, cylindrical horn with concentric insert and conical, cylindrical horn with concentric insert using finite element analysis. He concluded that the horn with a concentrically attached tool insert gave a satisfactory result during the machining. To enhance the productivity of the ultrasonic machining machine (USM), a double conical horn was studied by Vinod Yadav et al. [105]. This included both static and dynamic analysis of the horn. Further, the low frequency horns like blocked or slotted horns had been discussed by Cardoni et al. [106]. Finite element analysis of commercial horns like conical, stepped horns were analyzed using Ansys® and the natural frequency and amplitude were found to be closer with the commercial horns [107]. The finite element method includes modal analysis to find the natural frequency of the horn and harmonic response analysis to find the amplification ratio. Additionally, finite element analysis for the stepped type horn for making double flange by COMSOL® software and fabrication of the same were performed by Shu and Chen [108]. Since in the ultrasonic cutting process, the amplitude of the vibration plays a major role in reducing the cutting force, therefore, horns with high magnifications like stepped and Bezier type horns were assessed. Nguyen et al. [109] compared the amplification of a Bezier type horn and Catenoidal type horn. The authors concluded that the increase in amplification was 62% compared to the latter one.

2.4 Finite Element Analysis

During machining, there are complex processes occur at the shear zone as well as rake face, secondary zone where high strain rate and temperature are observed. Since, it is not an easy situation to study the flow stress, friction characteristics, tool wear rate using repetitive experiments, finite element method is a powerful numerical method to predict the process variables like stress, and tool wear with accuracy to improve the overall productivity [110, 111]. As far as thermal effects are concerned, cutting temperature distribution is a most desired factor which needs to be accurately predicted to analyze wear rate, tool life, thermal stress and tool chipping to identify the optimum cutting conditions, tool design, and coating to improve the cutting ability.

There are two major numerical formulations of finite element method, such as Eulerian and Lagrangian. Mostly, Lagrangian method is used for solving machining problems due to several advantages of this method over the latter [112]. Umbrello et al.

[113] investigated the turning of titanium alloy, Ti-6Al-4V using Deform 2D® to study the cutting forces, chip morphology and segmentation in chip considering Johnson-Cook's equation as a nonlinear material flow stress. Finite element modelling of turning of titanium was assessed by Li and Shih [114]. The model was prepared using the AdvantEdge® software to compare the cutting forces and chip thickness results with measured data to validate the model. There has been a comparison of the degree of accuracy of different commercially available software packages like MSC Marc®, AdvantEdge® and Deform 2D® [115]. The authors concluded that the simulation will not correlate with the experimental results until there is a proper selection of friction model, separation criteria, and material flow stress. Hua and Shivpuri [33] prepared an isothermal rigid-viscoplastic finite element simulation of turning of Ti-6Al-4V to predict the chip morphology and segmentation. Further, the model was validated with the experimental results. Schulze and Zanger [116] studied the effect of various Johnson- Cook constants on the surface integrity of Ti-6Al-4V. Ali et al. [117] found out optimum parameters for high speed cutting of Ti-6Al-4V using ABAQUS® software. To investigate the flow softening conditions on the output responses like chip morphology, segmentation during the turning of Ti-6Al-4V, Karpat [118] introduced a modified material flow stress to validate the simulation results. Calamaz et al. [119] used a modified constitutive material model to study the shear band formation, chip morphology along with cutting and feed forces. To simulate the model, the authors used Forge® software. Ma et al. [60] prepared a finite element model using AdvantEdge® to assess the effect of microgrooves present on the cutting insert on the cutting responses like cutting forces and chip-tool contact length. Additionally, to prepare optimum models and to validate with several cutting responses, several researchers formulated and taken Johnson- Cook's material constants [113, 120-123]. In early works, some researchers investigated turning models to achieve steady state cutting temperature and tool temperature for conventional turning using global heat transfer coefficient, suggesting friction model with different heat transfer coefficient [124, 125].

There were several 2D and 3D models proposed for ultrasonic vibration assisted turning using finite element method to investigate the intermittent characteristics of this process. Mitrofanov et al. [73, 77-79] prepared a thermo-mechanical and transient finite element model using MSC Marc® for both the cutting process to study the process occurring at the tool-chip interface, cutting temperature distribution, effect of cutting

parameters like velocity, feed, depth of cut and lubricant on the cutting responses. To analyze the reduction in cutting forces during UVAT process of Inconel 718, finite element model using MSC Marc® was prepared and validated [15, 81, 86, 89, 126]. Muhammad et al. [87] developed a 3D finite element model for oblique turning and hot ultrasonically assisted turning (HUAT). The model described the effect of cutting and vibration parameters on the cutting forces and tool temperature. The advantages of HUAT over ultrasonic assisted turning and conventional turning were analysed in the finite element analysis. Khajehzadeh et al. [75] prepared a 3D thermo-mechanical model using ABAQUS®. The authors studied the temperature evolution in the tool face and interface zone, further, validated the model with the experimental results. The effect of coated tool and uncoated tool on the cutting force was assessed in the model. Patil et al. developed a thermo-mechanical 2D model for UVAT of Ti-6Al-4V [92] and validated comparing with the experimental forces, temperature. The effect of friction coefficient was assessed in this model with the prediction of strain rate and stress generation.

2.5 Research Gaps

From the above literature review, the following gaps are identified that needs further research.

- Several research works have been done on solid horns with single or uniform body. An optimum horn design with flexible attachments has not yet mentioned by researchers.
- Although several models have been prepared for CT of titanium alloy, model preparation for UVAT of titanium alloy is very few, requires further research.
- Different researchers has discussed the thermal responses during UVAT modelling without considering steady state phenomenon, which is a major concern for a thermal model.
- Effect of UVAT on tool life applied to Ti-6Al-4V workpiece has not been explored.
- Few works have been suggested on the machinability of Ti-6Al-4V using UVAT which requires more research.

2.6 Novelty in the Present Work

- A flexible acoustic stepped type horn is designed and analyzed using finite element analysis with commercially available Ansys v15® FEM software.
- The horn is fabricated based on the finite element analysis and tuned with the ultrasonic system.
- The machinability of Ti-6Al-4V regarding cutting force reduction, improved surface finish with tool life enhancement is done during the UVAT process.
- A 3D thermo-mechanical finite element model is prepared to investigate the UVAT process and the effect of process parameters on the output responses like tool temperature, stress generation and interface temperature.

2.7 Closure

The comprehensive literature review states that the titanium alloy, Ti-6Al-4V has wide range of application in various industries. To meet the machining issues enhancing the machinability of the hard to cut alloys, novel machining processes like ultrasonic vibration assisted turning should be implemented and investigated. Researches on acoustic horn show that there are rigorous researches to optimize the acoustic horn of single body type. Due to continuous supply of ultrasonic vibration, there is a chance of wear and tear of the smaller end of the horn. Therefore, there is a requirement for a flexible horn with optimum amplification. In simulation modelling, several works have been performed for CT of titanium alloy, but model preparation for UVAT of titanium alloy is very few, requires further research. Several studies have been developed to analyze the thermal related responses like tool and interface temperature, but investigation on steady state temperature evolution during UVAT process are yet to be explored.

Chapter 3

Design, Analysis and Fabrication of Acoustic Horn

The present chapter explains various acoustic horns or sonotrode used in the ultrasonic vibration assisted turning (UVAT) system. It has been observed that the effectiveness of this process is more prominent when the amplification of tool vibration amplitude is relatively high. The stepped type horn and Bezier type horn possess the similar amplification enhancement characteristic compared to the other types. Due to ease of manufacturing, the stepped type horn is more focused in the present chapter. The governing equation defining the ultrasonic wave propagation in a solid horn has been constructed. Additionally, the chapter defines a flexible stepped type horn based on the finite element method.

3.1 Acoustic Horn

Acoustic horn or sonotrode is the fundamental part of an ultrasonic vibration assisted machining, transmitting the low vibration energy to the required tool or cutting edge during the machining process. The horns are made of metals that have high fatigue strengths and low acoustic losses. Different types of horns and commonly used horns (Figure 3.1), like cylindrical, conical, exponential, stepped, and Bezier horns have been discussed by several researchers in the past.

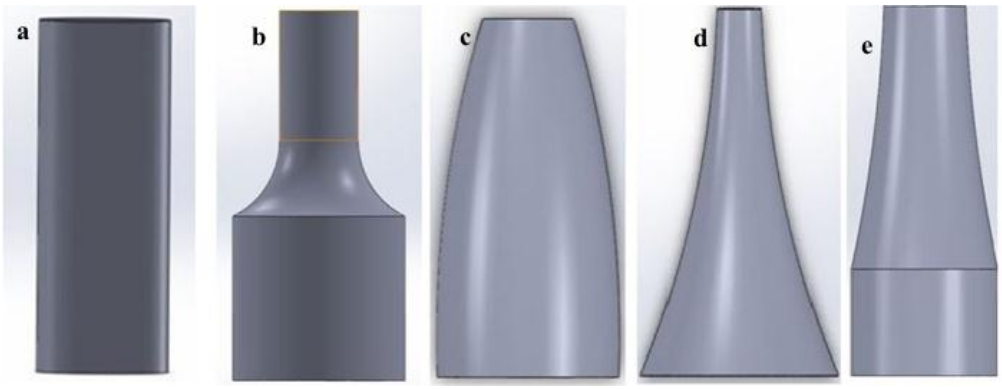

Figure 3.1 (a) Cylindrical (b) Stepped (c) Gaussian (d) Catenoidal (e) Bezier Type horn

Since, the advantages obtained from the ultrasonic vibration assisted manufacturing is due to the intermittent motion of the cutting insert attached to the horn, generally, the stepped and Bezier type horn possessing higher amplification compared to the other horns, are used [36]. Selection of geometric shape of sonotrode depends on technological operation, amplification factor and ease of manufacturing. Bezier and stepped horns have almost same amplification factor [36]. However, to fabricate a Bezier horn, one may require employment of copy turning or NC machine which may not be available [104]. So, stepped type is chosen over Bezier type. Further, stepped type horn has been extensively used and investigated due to ease of manufacturing and higher amplification [103, 127].

3.2 Acoustic Wave Equation

The plane wave equation can explain the propagation of the ultrasonic wave in the solid medium. The favorable ultrasonic vibration required to propagate through the horn is the longitudinal mode of vibration.

Let's consider a non-uniform cylinder with a longitudinal mode as shown in the Figure 3. 2. The direction of vibration is along the axis of the cylinder. A small element of 'dx' is chosen for the analysis.

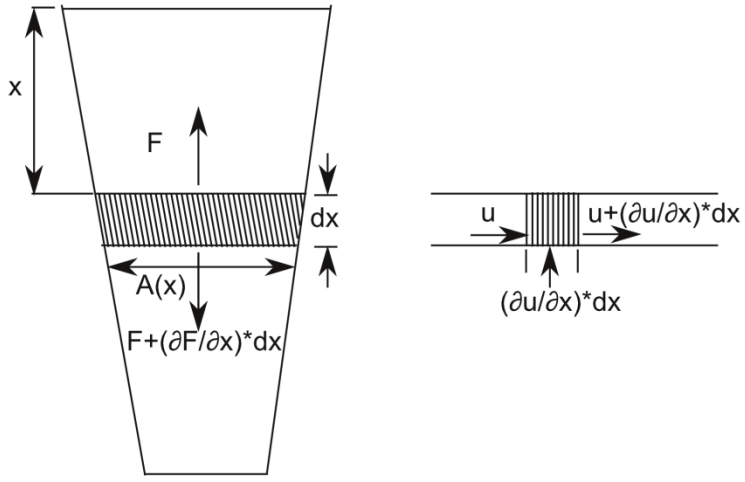

Figure 3.2 Non-uniform cylinder with a small element, dx [101]

Let 'u' be the displacement at a distance x from the origin or reference, and it becomes $\left(u+\frac{\partial u}{\partial x}dx\right)$ at a distance of $(x+dx)$. So the total displacement due to change in the position can be written as

$$\text{Total displacement, } \left(\left(\mathrm{u}+\frac{\partial \mathrm{u}}{\partial \mathrm{x}}\mathrm{dx}\right)-\mathrm{u}\right)=\frac{\partial \mathrm{u}}{\partial \mathrm{x}}\mathrm{dx} \tag{2}$$

The strain of the element is given by

$$\text{Strain, } \varepsilon=\frac{\frac{\partial u}{\partial x}dx}{dx}=\frac{\partial u}{\partial x} \tag{3}$$

Let, A (x) be the cross-sectional area of the element vary with the position of the element

ρ is the density of the material, E is the modulus of elasticity of the material, F is the force acting axially on the cylinder, Net force acting on the element is given by,

$$\left(F+\frac{\partial F}{\partial x}dx\right)-F=dm*\frac{\partial u^2}{\partial t^2}=\rho*A(x)*dx*\frac{\partial u^2}{\partial t^2}$$

$$\Rightarrow \frac{\partial F}{\partial x}dx=\rho*A(x)*dx*\frac{\partial u^2}{\partial t^2} \tag{4}$$

Where, dm is the mass of the element, $\frac{\partial u^2}{\partial t^2}$ is the acceleration of the element.

Further, substituting the value of strain from Eq. (3), the stress generated on the element due to vibration is given by

$$\text{Stress, } \sigma_x=E*\varepsilon=E*\frac{\partial u}{\partial x} \tag{5}$$

Since, force, $\mathrm{F}=(\text{Stress},\sigma_x)*(\text{Crosssectional area, A}(\mathrm{x}))$, therefore, Eq. (4) can be written as.

$$\frac{\partial(\sigma_x*A(x))}{\partial x}dx=\rho*A(x)*dx*\frac{\partial u^2}{\partial t^2}$$

$$\Rightarrow A(x)\frac{\partial \sigma_x}{\partial x}dx+\sigma_x\frac{\partial A(x)}{\partial x}dx=\rho*A(x)*dx*\frac{\partial u^2}{\partial t^2}$$

$$\Rightarrow A(x)*E*\frac{\partial^2 u}{\partial^2 x}dx+E*\frac{\partial u}{\partial x}*\frac{\partial A(x)}{\partial x}dx=\rho*A(x)*dx*\frac{\partial u^2}{\partial t^2}$$

$$\Rightarrow \frac{\partial u^2}{\partial t^2}=\frac{E}{\rho*A(x)}*\frac{\partial u}{\partial x}*\frac{\partial A(x)}{\partial x}+\frac{E}{\rho}*\frac{\partial^2 u}{\partial^2 x}$$

$$\Rightarrow \frac{1}{C^2}\frac{\partial u^2}{\partial t^2}-\frac{1}{A(x)}*\frac{\partial u}{\partial x}*\frac{\partial A(x)}{\partial x}-\frac{\partial^2 u}{\partial^2 x}=0 \tag{6}$$

$$\left(\text{where, } C^2 = \frac{E}{\rho}\right)$$

The displacement can be represented by,

$$u(t) = M\cos\omega t + N\cos\omega t \tag{7}$$

Where, ω is the angular velocity, M and N are constants. So, the acceleration can be defined as,

$$\frac{\partial^2 u}{\partial^2 t} = -\omega^2 u \tag{8}$$

The Eq. (6) can be written as,

$$\frac{\partial^2 u}{\partial^2 x} + \frac{1}{A(x)} * \frac{\partial u}{\partial x} * \frac{\partial A(x)}{\partial x} + \frac{\omega^2}{C^2} * u = 0 \tag{9}$$

The above Eq. (9) represents the one-dimensional plane wave equation.

3.3 Cylindrical Horn

Cylindrical horn or uniform horn is the basic horn used in ultrasonic vibration assisted manufacturing. The wave equation propagating through this horn can be found out by making cross sectional area constant shown in the Figure 3.3 and can be written as,

$$\frac{1}{C^2}\frac{\partial u^2}{\partial t^2} - \frac{\partial^2 u}{\partial^2 x} = 0 \tag{10}$$

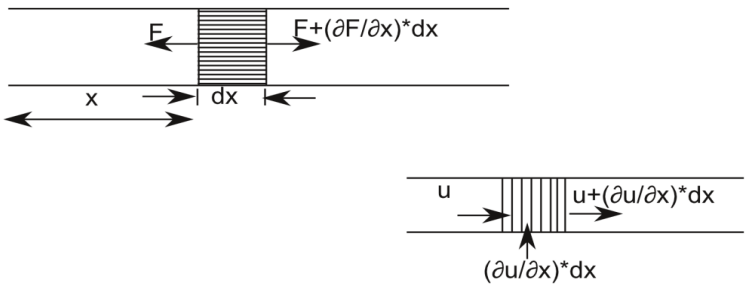

Figure 3.3 Longitudinal vibration propagation in cylindrical horn with uniform area

The solution equation can be written as,

$$U(x,t) = X(x) * T(t) \tag{11}$$

$$\text{Or, } X\frac{\partial^2 T}{\partial t^2} = T * C^2 * \frac{\partial^2 X}{\partial x^2} \tag{12}$$

Let, $$\frac{C^2}{X} * \frac{\partial^2 X}{\partial x^2} = \frac{1}{T} * \frac{\partial^2 T}{\partial t^2} = -P^2$$

or, $$\frac{\partial^2 X}{\partial x^2} + \frac{P^2}{C^2} * X = 0, \tag{13}$$

and, $$\frac{\partial^2 T}{\partial t^2} + P^2 * T = 0 \tag{14}$$

The general solution for Eq. (13) and (14) are given as,

$$X(x) = A\sin\left(\frac{P}{C}\right)x + B\cos\left(\frac{P}{C}\right)x \tag{15}$$

and, $$P(t) = A_1 \sin Pt + B_1 \cos Pt \tag{16}$$

where, A, B, A_1 and B_1 are the constants and can be found out applying boundary conditions and $P = 2\prod f$ is angular frequency

The general solution for the Eq. (11) can be written as,

$$U(x,t) = \sum_{n=1}^{\infty}\left[A\sin\left(\frac{P}{C}\right)x + B\cos\left(\frac{P}{C}\right)x\right] * \left[A_1 \sin Pt + B_1 \cos Pt\right] \tag{17}$$

When the horn is in the free- free conditions without any external load, the boundary conditions are,

$$\left.\begin{aligned}\left(\frac{\partial u}{\partial x}\right)_{x=0} &= 0\\ \left(\frac{\partial u}{\partial x}\right)_{x=l} &= 0\end{aligned}\right\} \tag{18}$$

Applying the boundary conditions on the general solution, we will get,

$$\sin\left(\frac{P}{C}\right) * l = 0 = \sin(n\prod) \tag{19}$$

or, $P = \frac{n\prod C}{l} = \frac{n\prod}{l}\sqrt{\frac{E}{\rho}}$, n, order of the mode= 1, 2, 3, 4…

$$\text{or, } P = 2\prod f = \frac{n\prod}{l}\sqrt{\frac{E}{\rho}} \tag{20}$$

So, natural frequency for n=1 is,

$$f = \frac{1}{2l}\sqrt{\frac{E}{\rho}} \tag{21a}$$

$$\Rightarrow l = \frac{1}{2f}\sqrt{\frac{E}{\rho}} = \frac{C}{2f} = \frac{\lambda}{2} \tag{21b}$$

The above Eq. (21b) depicts that the resonant horn length (l) for a uniform cylindrical horn is the half of the wavelength of the vibration. The amplification is uniform along the horn length due to unchanging displacement at both the ends.

3.4 Stepped Type Horn

Stepped type horn is an adjustment of the uniform cylindrical horn with a larger diameter of D_1 and smaller diameter of D_2 as shown in Figure 3.4.

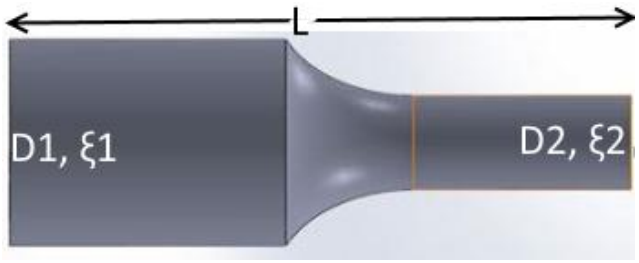

Figure 3.4 Stepped type horn

Since the diameter changes, according to the conservation of momentum, the velocity at the end with smaller diameter end should be greater than the other end. That results amplification at the smaller diameter and can be expressed as follows,

$$\frac{\xi_2}{\xi_1} = \frac{A_1}{A_2} = \left(\frac{D_1}{D_2}\right)^2 \tag{22}$$

Where, ξ_1 and ξ_2 are the amplitudes at the larger and smaller diameter ends respectively. A_1 and A_2 are the area of the larger diameter (D_1) end and smaller diameter (D_2) end respectively.

For stepped horn, the resonant length can be divided into L_1 and L_2 with a radius of curvature (R) of the area where diameter changes from D_1 to D_2. The following equation can express the resonant length,

$$L = k_1\left(\frac{C}{4f}\right) + k_2\left(\frac{C}{4f}\right) \tag{23}$$

where, L is the resonant length

C is the sound velocity in the horn material,

'f' is the natural frequency of the vibration

K_1 and K_2 are the correction factors and taken as unity.

The area where change occurs is called nodal point with minimum displacement and maximum stress.

3.5 Finite Element Modelling of Acoustic Horn

Finite element modelling is an analytical method used by the researchers to predict, analyze, and solve the physical problems. The analysis is not correct until the experimental results validate it. The principle of FEM depicts that the accuracy of a solution during the analysis will be more if the mesh size is infinitely small. Modelling of the problem with an optimum mesh size is a key criterion in this analysis. In the present analysis, quadrilateral elements have been chosen; that generates more accurate results compared to the other element shapes [81]. The analysis is done using the commercial package Ansys v15® [128]. The finite element analysis includes three basic steps, such as (a) Pre-processor, (b) Simulation, and (c) Post Processor. In pre-processor, input for the simulation like geometry design and material assignment, mesh generation, boundary conditions are assigned. The detailed geometry and meshed model are shown in Figure 3.5 (a, b).

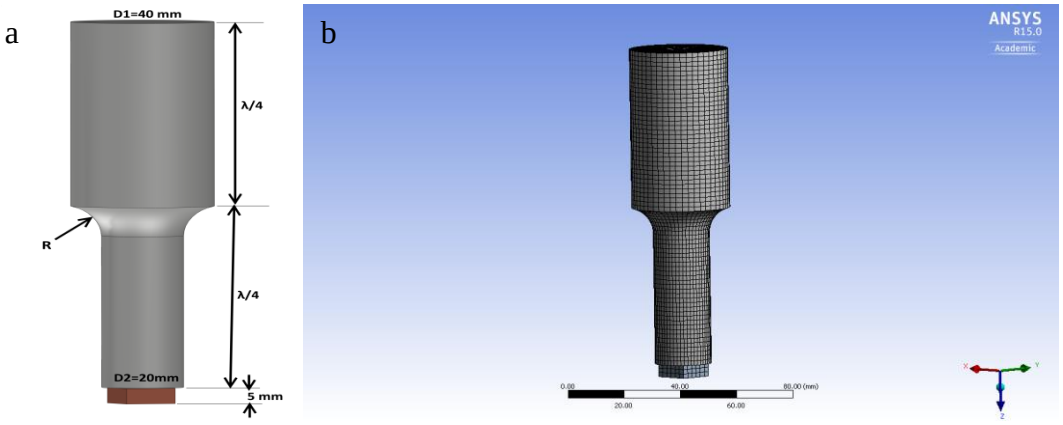

Figure 3.5 (a) Stepped type horn, (b) Meshed geometry of the stepped horn

In the present work, the stainless steel 304 grade is chosen as the horn material with a working frequency of 20 kHz. Stainless steel offers good characteristics for the use of ultrasonic horns. They exhibit high strength, stiffness, excellent wear resistance and corrosion resistance. They may be used over wide range of temperature. These are easily available and cheaper as compared to Ni alloys and Ti alloys. Further, due good machinability property during fabrication, SS 304 was chosen over other horn material [65]. The properties of Stainless Steel, SS 304 are given in Table 3.1.

Table 3.1 Material properties of SS 304 [129, 130] and cutting insert [131]

Property	SS304 Horn	Tungsten Carbide
Density	8000 kg/m^3	15680 kg/m^3
Elastic modulus	193 MPa	605 MPa
Poisson's ratio	0.3	0.25
Sound velocity	4912 m/sec	6212 m/sec
Fatigue strength	269 MPa	-
Damping ratio	0.001-0.002	-

3.5.1 Modal analysis

Modal analysis deals with the free vibration analysis of a body/ structure. The purpose is to find the shapes and frequencies at which the structure will amplify the effect of a load. The governing equation to explain the free vibration of a body using FEM is given by the following Eq. (24) [102].

$$M\ddot{U} + B\dot{U} + KU = 0 \tag{24}$$

where, M, B, and K are the mass, damping and stiffness matrix respectively. $\ddot{U}, \dot{U}$ and U are the acceleration, velocity and displacement vector of the horn vibration respectively.

Since, the horn material possesses low damping capacity, damping factor, B can be neglected, and the equation can be written as follows,

$$M\ddot{U} + KU = 0 \tag{25}$$

Modal analysis is a linear analysis, any nonlinearities such as plasticity and contact elements, are ignored, even if they are defined. The analysis was performed in the user

interface provided in Ansys workbench. The modes were extracted by Block Lanczos algorithm.

There are numbers of resonant frequencies recorded within the range of 15000 Hz to 30000 Hz. The longitudinal axial mode shape of UVAT is found at 20005 Hz as shown in Figure 3.6. There are also other modes; twisting mode at 25465 Hz and bending mode at 27253 Hz as shown in Figure 3.7 and 3.8 respectively. It is apparent from Figures 3.7 and 3.8 that these two modes are results of superimposing two or more longitudinal modes in different directions. This is an undesirable phenomenon which can jeopardize the advantages of UVAT by hampering the accuracy and surface finish in turning operation. Hence, the first longitudinal mode is preferred and considered for UVAT.

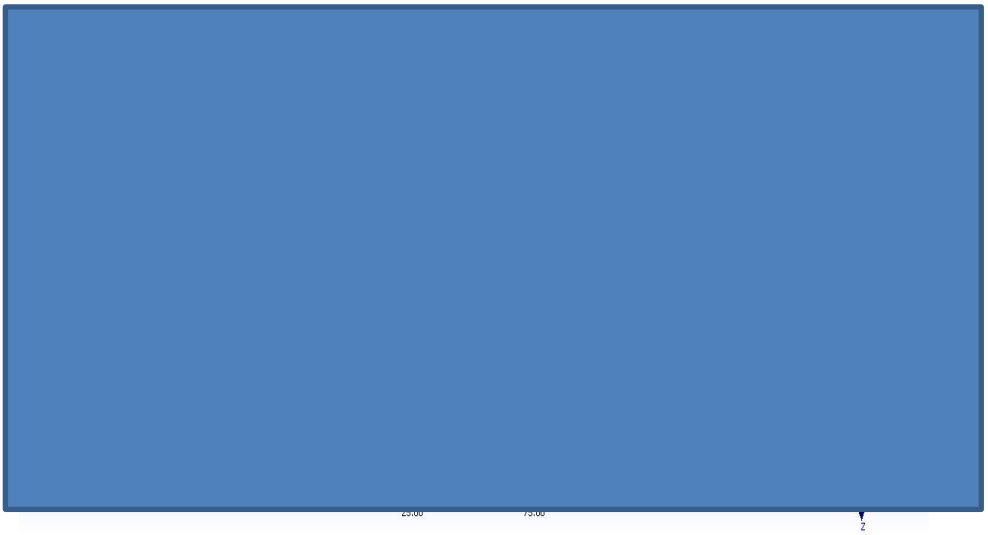

Figure 3.6 Longitudinal mode (1st mode) of the horn with frequency, 20005 Hz

Figure 3.7 Twisting mode (2nd mode) of the horn with frequency, 25465 Hz

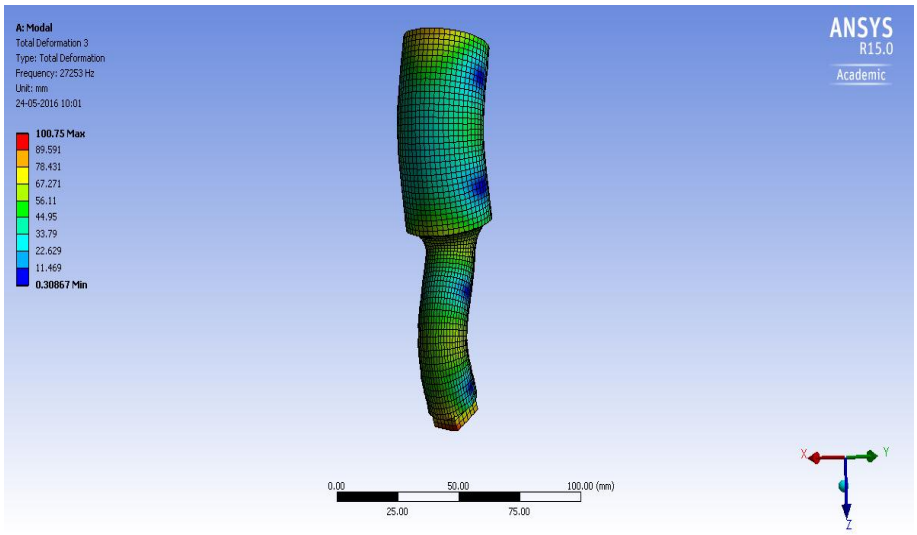

Figure 3.8 Bending mode (3rd mode) of the horn with frequency, 27253 Hz

3.5.2 Harmonic analysis

Harmonic analysis is used to determine the response of the structure under loading at a given frequency. It predicts the dynamic behavior of the structure verifying whether the structure is sustainable to resonance, fatigue effect and other harmful effects. As per the equipment specification, an output of 10 µm from the transducer is 1.5 times amplified at the booster end converting to 15 µm. This displacement amplitude is given as a function of the cyclic load at the input or larger diameter (35mm) of the horn as shown in Figure 3.9a. The experimental setup (Figure 3.9b) to check the horn consists of an ultrasonic generator, transducer, booster, and the horn.

Figure 3.9 (a) Load applied as a function of displacement, 0.015 mm, (b) Experimental set up for tuning of horn

Based on the analytical calculation, the horn was manufactured and checked for the tuning using the ultrasonic generator Telsonic® SG-22 of 2000W and 20 kHz capacity. Initially, the horn is tuned to 19580 Hz. After a few trials of length shortening, the horn was tuned to 20 kHz with no load condition. The final effective length of the horn is found to be 125.5 mm.

3.5.3 Mesh independence test

The variation of natural frequency due to the chosen number of elements during the mesh generation and solution is the main concern with respect to the accuracy of the result and computational time. When the number of an element is less, results are showing a significant error because of inaccurate approximation. The Figure 3.10 shows the mesh convergence and 20628 numbers of 3D elements (quadrilateral type) are taken to conserve computation time without hampering the accuracy of the result.

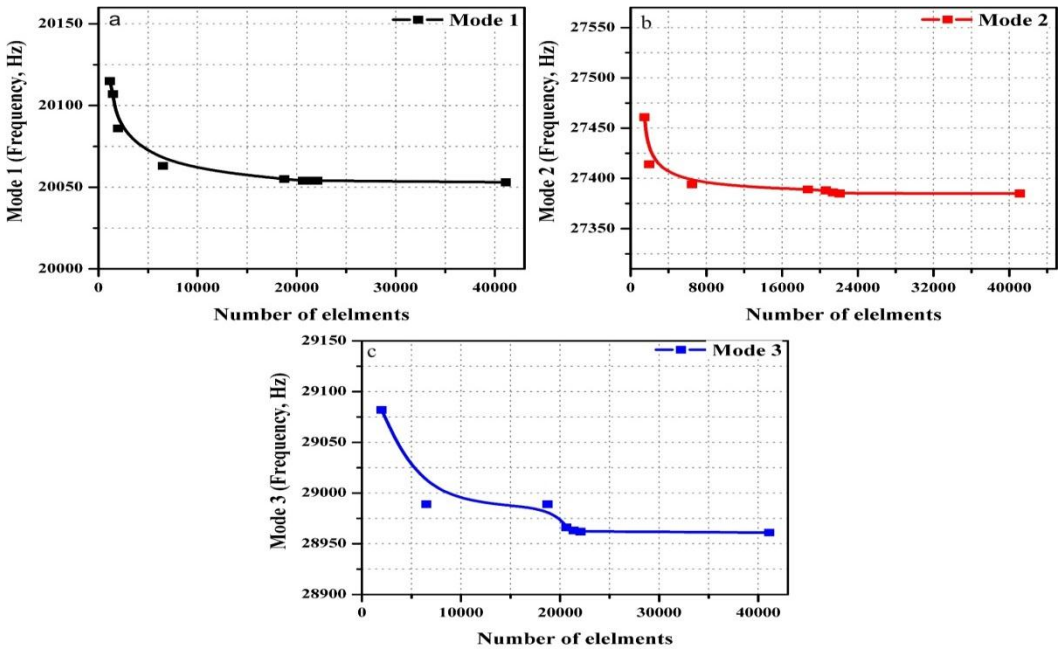

Figure 3.10 Mesh independence test

3.6 Comparison of Analytical and Experimental Results

Based on the modal and harmonic analysis, the horn was manufactured, and the actual length of the stepped horns was found to be 125.5 mm. The fabricated horn with the dimensions is shown in Figure 3.11.

Figure 3.11 Fabricated stepped horn with dimensions

Resonant length corresponding to the operating frequency, 20 kHz ± 500 Hz obtained from both analytical and experimental methods are presented in Table 3.2. The amplification results obtained from theoretically and analytically have been compared and given in Table 3.3. From the harmonic analysis; it can be concluded that the results quite satisfy the theoretical calculation. Further, the directional deformation from the FEM is shown in Figure 3.12 (a, b) indicating a nodal point at a distance of 58 mm from the bigger end.

Table 3.2 Comparison of resonant lengths of the stepped horn

Results	Analytical (mm)	Experimental (mm)	Error (%)
Resonant length	124	125.5	1.19

Table 3.3 Comparison of amplification ratio

Results	Theoretical	Analytical from FEM	Error (%)
Amplification ratio	3.0625	3.0110	1.68

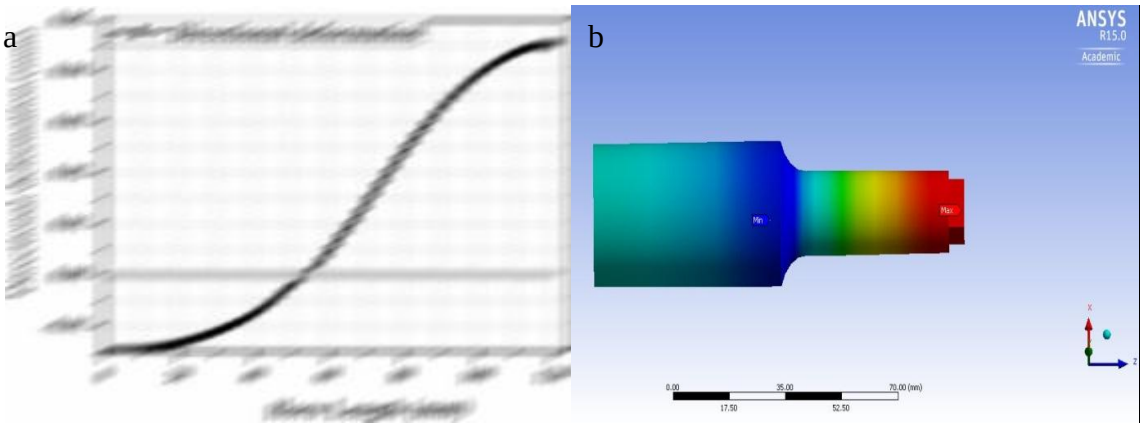

Figure 3.12 (a) Amplitude amplification corresponding to the length of horn (b) Directional deformation along the axis of the stepped horn

3.7 Horn Parameters on the Natural Frequency

There are mainly two parameters which affect the natural frequency of a stepped type horn. Those are resonant length and radius of curvature. The effects are shown in Tables 3.4 and 3.5. From the result, we can conclude that the length of the horn has an inverse effect on the natural frequency. Also, as the radius of curvature increases, the natural frequency gets increased. So, adjusting these parameters in a model, we can get the desired natural frequency with the final horn geometry.

In a single or uniform body, due to the vibration, the end of the horn subject to wear and tear that affects the tuning after repeated use as observed and shown in Figure 3.13. Therefore, a flexible acoustic stepped type horn has been proposed to prevent from throwing out the complete horn due to wear and tear avoiding wastages of material, which will be more cost effective.

Table 3.4 Effect of length (L) on natural frequency

Length, L (mm)	Radius of curvature, R (mm)	Frequency, f (Hz)
124.5	10	19956
124	10	20005
125	10	19775
126	10	19611

Table 3.5 Effect of radius of curvature (R) on natural frequency

Length, L (mm)	Radius of curvature, R (mm)	Frequency, f (Hz)
124	0	19146
124	1	19231
124	5	19606
124	10	20005
124	15	20409

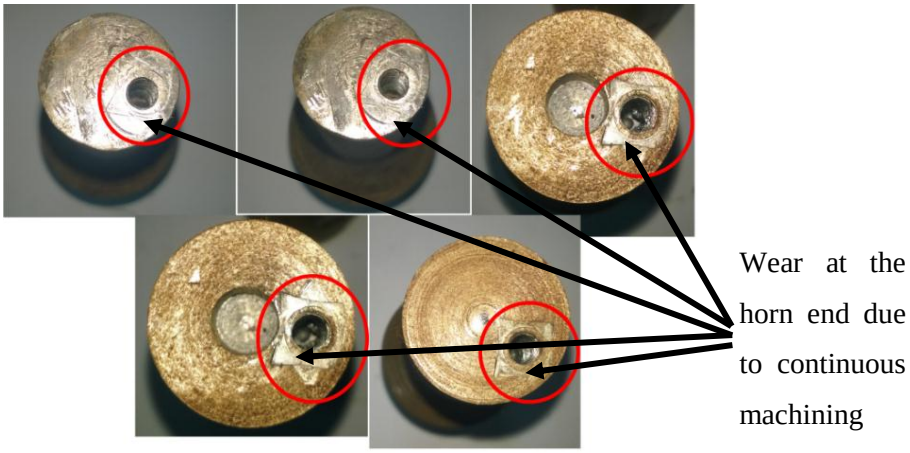

Figure 3.13 Wear and tear of the horn end due to repetitive use

3.8 Proposed Horn Design

The proposed horn is a modification of stepped horn and consists of an M12 bolt head onto which, the cutting insert is tightened with the help of a screw. The detailed design of horn with the booster is depicted in Figure 3.14 (a, b). As discussed, due to the impact load during repetitive vibration, the horn end starts tearing and subsequently changes the natural frequency (Figure 3.13). As M12 bolt is attached to the horn end, it can be removed out without changing the complete horn. Further, analyses (Modal and Harmonic) are carried out taking booster combined with the proposed horn. The properties of the materials used for booster, horn, bolt, and insert are Ti-6Al-4V, stainless steel (SS 304 grade), mild steel, and tungsten carbide respectively (Table 3.6).

Figure 3.14 (a) Booster dimensions, (b) Assembly of horn with booster

Table 3.6 Material properties used in the proposed horn and booster [2, 129, 131, 132]

Property	Ti-6Al-4V	SS304 Horn	Mild steel bolt	Tungsten Carbide
Density	4430 kg/m^3	8000 kg/m^3	7780 kg/m^3	15680 kg/m^3
Elastic modulus	113 GPa	193 GPa	210 GPa	605 GPa
Poisson's ratio	0.342	0.3	0.3	0.25
Sound velocity	5050 m/sec	4912 m/sec	5195 m/sec	6212 m/sec
Fatigue strength	510 MPa	269 MPa	-	-
Yield Stress	-	202 MPa	-	-

3.8.1 Modal analysis results

The assembly of the booster and the proposed horn was undergone modal analysis using the free vibration approach. The longitudinal mode was found at a frequency of 20008 Hz. The three different modes obtained during modal analysis are depicted in Figure 3.15. The analytical length was compared with the fabricated length of the assembly with an error percentage of 1.63 % given in Table 3.7 (for longitudinal mode).

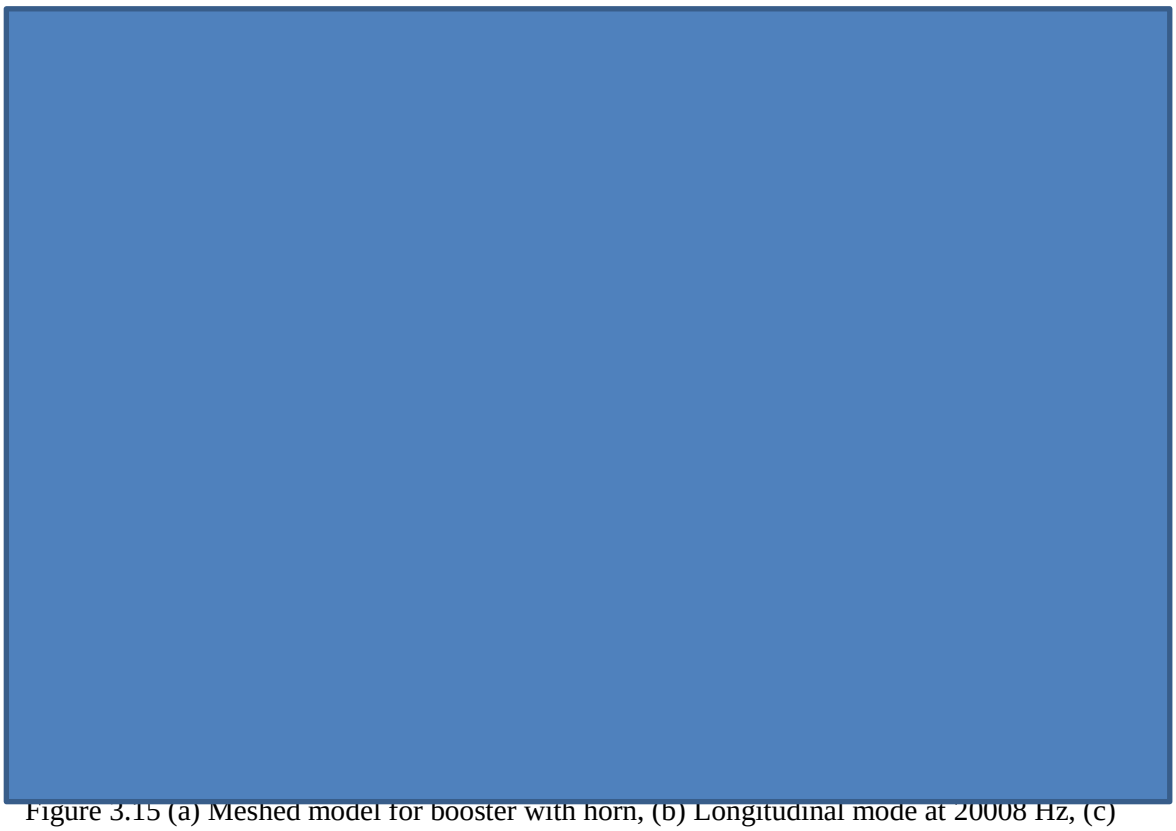

Figure 3.15 (a) Meshed model for booster with horn, (b) Longitudinal mode at 20008 Hz, (c) Bending mode at 20800Hz and (d) Twisting mode at 23485 Hz

Table 3.7 Comparison of lengths obtained analytically and experimentally

Results	Analytical (mm)	Experimental (mm)	Error (%)
Resonant Length (Only Horn)	120.73	125	3.40
Resonant length (Booster + Horn)	256.23	260.5	1.63

3.8.2 Harmonic analysis results

The primary results obtained from the harmonic analysis are amplification ratio and dynamic characteristics of the model. The dynamic results include stress generation and its concentration along the length of the model. A comparative analysis is represented in the following Table 3.8.

Table 3.8 Comparison of amplification ratio

Results	Theoretical	Analytical	Error (%)
Amplification ratio	3.0625	2.991	2.33

The amplification was found to be almost three times of the input amplitude supplied at the horn end and its variation with location represented in Figure 3.16 (a, b). From the analysis, it was confirmed that the amplitude was minimum at the nodal points where the diameter for booster and horn changed. Further, the maximum amplitude occurred at the cutting insert with a value near to 45 μm.

The dynamic characteristics of the proposed horn are the main concern for the life of the horn. The stress concentration at the area, where the horn diameter changes, is maximum for the stepped horn and the value should be under the fatigue strength or endurance limit of the material, SS 304. From the harmonic analysis, the equivalent stress (Von-mises stress) is found to be 225MPa, which is lower than the fatigue strength (269 MPa) as of the horn material. The stress concentration variation along with the axis of the horn and normal to the horn has been shown in Figure 3.17. Based on the modal and harmonic analyses, the proposed flexible stepped type horn was fabricated as given in Figure 3.18.

From the figure, it is substantiated that the stress concentration is high at the portion where the diameter changes. Therefore, the analysis can be very informative to the manufacturer or industry regarding the horn design without any material loss before hand.

Figure 3.16 (a) Amplitude amplification corresponding to the length of booster and horn (b) Directional deformation along the axis of the assembly

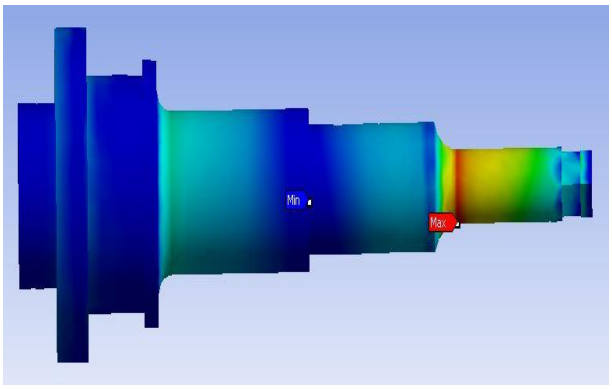

Figure 3.17 Equivalent stress magnitude along the axis of the assembly

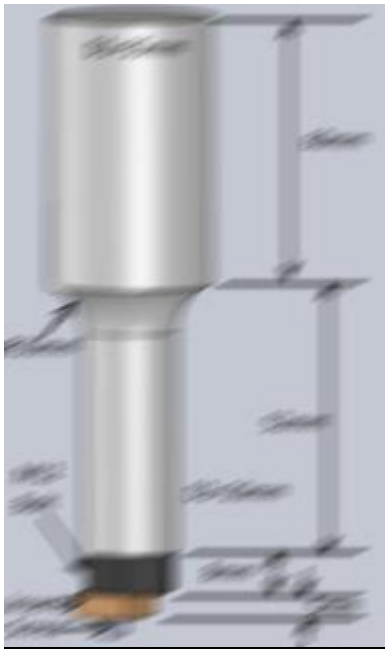

Figure 3.18 Fabricated flexible stepped horn with dimension

3.9 Conclusions

The experimental, mathematical, computational modeling of the single body stepped horn, and a flexible stepped horn were carried out. The following conclusions can be drawn from the observations:

a. Unlike a conventional design of horn i.e. single body horn design, a flexible type has been proposed and analyzed using finite element method.
b. The resonant horn length was found out from the numerical method corresponding to the operating ultrasonic frequency, 20 kHz ± 500 Hz and compared with the experimental results. The horn lengths for single uniform stepped horn, and

flexible horn were found to be 125.5mm and 125mm with error percentages of 1.19 % and 3.40 % respectively.

c. From the free vibration analysis, different modes were found out, and grid independence test was performed to get an optimum number of elements, i.e. 20628 to conserve computation time without hampering the accuracy of the result.
d. Dynamic analysis results confirm an allowable stress concentration range for different stresses during the cyclic loading that is below the fatigue strength of the proposed horn material. Additionally, the maximum stress is observed at the nodal points.
e. Further, both theoretical and numerically obtained amplification ratios were compared. The error of 1.68% and 2.33% are found for conventional stepped horn and flexible horn respectively. It substantiates that finite element method is a powerful tool to model and analyze the prototype before the actual fabrication, which is cost saving and economical.

Chapter 5

Numerical Modelling and Comparison of Results

The present chapter focuses on building a thermo-mechanical model for CT and UVAT to investigate the mechanism, effect of controlling parameters and prediction of output responses. The analysis, a three-dimensional finite element model, assists in understanding the CT and UVAT processes focusing on the cutting zone, material behavior, and outputs. Further, model validation was carried out selecting proper friction model, flow stress, and other thermal conditions.

5.1 Numerical Modelling

A 3D thermo-mechanical coupled finite element model was prepared to understand both the processes using the commercial FEM software Deform 3D® v10.2. The model is based on the Lagrangian incremental procedure with continuous remeshing criteria that allows processing the transient analysis. The present model accommodates the mechanical processes along with the temperature evolution, damage, stress generation, strain rate etc., which are thermally related to each other during the plastic deformation at the cutting zone. Also, it includes temperature dependent factors like thermal conductivity, density, specific heat, and material flow stress. Remeshing is an important criterion in the model that helps to continue the simulation process when there is a generation of distorted mesh at the cutting zone. The numerical model preparation and investigation can be classified in three steps [37] such as,

(i) Pre-processor
(ii) Simulation engine
(iii) Post-processor

5.1.1 Pre-processor

Pre-processor is the initial stage of a model preparation in which different input data are given to a graphical user interface (GUI) required for a simulation. Those input data particularly for turning operation can be listed as follows,

(i) Object definition

It includes the object models and geometries of individual parts like workpiece and cutting tool. Further, it allows scaling the size of geometry to meet the requirement of a physical problem.

(ii) Meshing

Finite element method calculates the complete problem by discretizing the complete geometry into small elements or mesh. The accuracy and predictability of a model depend on the meshing and its generation criteria. The present method allows us to mesh the objects into tetrahedral elements using a mesh window. Further, the meshing part incorporates remeshing criteria when there are distorted elements at the process zone, for instance, tool-workpiece interface zone in turning operation. It is a process of replacing distorted elements with undistorted elements interpolating the field variables like strain, velocity, damage, temperature, etc. from the old mesh to new mesh [37].

(iii) Material model

It includes the material assignment to the objects, identification of the object type (rigid, plastic, and elastic) and assignment of reference temperature to the objects. Additionally, the material assignment includes nonlinear material models such as Johnson-Cook material model, power law model, and Zerilli-Armstrong model, etc.. The physical and thermal properties like density, modulus of elasticity, hardness, thermal conductivity, melting temperature, specific heat capacity, and heat transfer coefficients, etc. are defined.

(iv) Inter-object condition

The main aim of this step is the selection of a proper friction model to process an accurate model. There are several types of friction models, for instance, shear friction model, Coulomb friction model, hybrid friction model, variable friction model, etc.

(v) Simulation controls

It defines the various types of solution and algorithms that can be assigned to the model assembling the input data. Further, the simulation time, steps, data collection, and saving can be controlled with simulation controls.

(vi) Boundary conditions

It includes all the kinetic and thermal boundary conditions associated with the physical problem. Particularly in tuning models, while assigning the cutting velocity, the workpiece surfaces are fixed expect the top surface reducing the degree of freedom. Thermal boundary conditions include assignment of heat sources, assignment of temperature and heat transfer constants to particular surfaces.

5.1.2 Simulation engine

The simulation of the model is carried out by the solution method assigned in the simulation control. Different solution methods are direct iteration, Newton-Raphson method etc. Further, the simulation results vary with the type of algorithm used in a model. Different algorithms can be used are Lagrangian algorithm, Arbitrary Lagrangian Eulerian algorithm, steady state algorithm etc. The simulation process can be observed in a simulation graphics window to study the output responses.

5.1.3 Post-processor

The simulation results are stored in the post-processor step in a database file (*.DB).The output responses like cutting force, temperature evolution, stress and strain generation, tool wear, and microstructure can be studied.

5.2 Model Preparation for CT and UVAT

The workpiece with a dimension of 5 mm in length x 1.5 mm in breadth x 0.5 mm in height was used as a plastic or deformable body. It was discretized into 20533 numbers of tetrahedral elements later increased to 23831 numbers due to remeshing with refined mesh at the cutting zone with an element size of 30 μm. The element size or number of elements is optimally chosen after performing a grid independency test (when it was found that there was no significant change in the results due to mesh numbers). The cutting tool was

modeled with a rake angle of zero degree and a nose radius of 0.08 mm using Solidworks® and imported as .stl format file. Due to high stiffness compared to the workpiece, the insert was considered as a rigid body. Further, it was discretized into 90048 tetrahedral elements with high mesh density near the cutting edge with the help of mesh window for improved accuracy. The meshed workpiece and the cutting tool are shown in Figure 5.1. To get the intermittent motion, the path of the cutting insert was modified and cutting tip velocity (V_t) was defined as the function of time unlike in conventional turning model as shown in Figure 5.2. The tool vibrates in the tangential direction with a frequency of 20 kHz and amplitude of 45 µm.

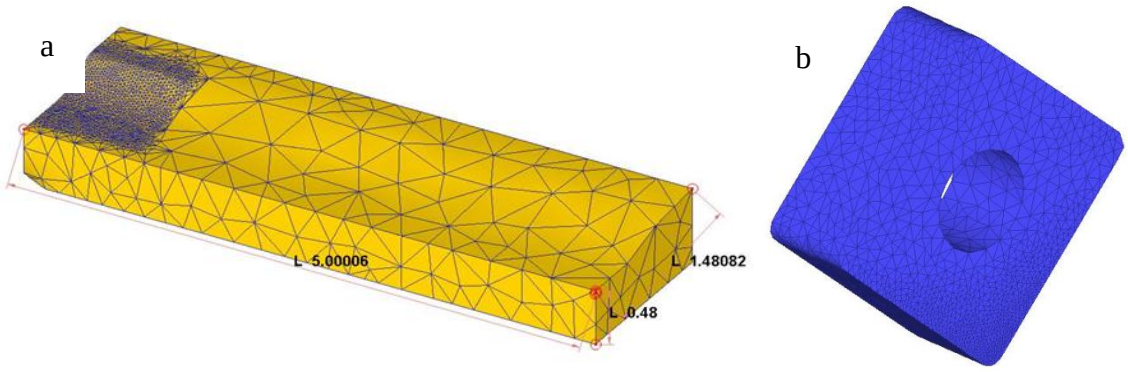

Figure 5.1 (a) Meshed Workpiece with dimension (b) Meshed cutting tool

Figure 5.2 Boundary conditions with tool movement as a function of velocity

Kinetic boundary conditions were provided on the bottom, right, and left surface of the workpiece keeping a free top surface and can be explained as follows.

$$V_X \mid_{ABCD} = V_X \mid_{EFGH} = 0,$$

$$V_Z \mid_{AFGD} = 0 ,$$

$$V_Y \mid_{ABCD} = V_Y \mid_{EFGH} = V_Y \mid_{AFDG} = V = 300 mm/\sec$$

The workpiece moves with a cutting velocity of V_c = 300 mm/sec that is below the critical velocity, or the maximum tool tip velocity (V_t) to process an effective ultrasonic vibration effect during the turning operation. The initial temperature was set as 20^0C and the top free surface was assigned with a convection coefficient constant (h_c) of 0.02 N/mm/sec/C [37]. Initial simulations of both the cutting processes were carried out with minimum cutting speed of 300 mm/sec, feed of 0.04 mm/rev and depth of cut of 0.14 mm.

A non-linear strain rate and temperature sensitive material model to describe the material behavior of Ti-6Al-4V was implemented using Johnson and Cook model [37] as shown in Eq. (33). The corresponding parameters in Eq. (33) show the dependencies of flow stress on strain, strain rate, and thermal softening respectively.

$$\sigma = \left[A + B\varepsilon^n\right]\left[1 + C\ln\left(\frac{\dot{\varepsilon}}{\dot{\varepsilon}_0}\right)\right]\left(\frac{\dot{\varepsilon}}{\dot{\varepsilon}_0}\right)^{\alpha}\left[D - ET^{*m}\right] \tag{33}$$

where, $T^* = \dfrac{T - T_r}{T_m - T_r}$

$\sigma, \varepsilon \,\&\, \dot{\varepsilon}$ are yield stress, plastic strain, and strain rate respectively. T_r and T_m are the room temperature and melting temperature of TI-6Al-4V respectively. The material coefficients are mentioned in the following Table 5.1.

Table 5.1 Material coefficients used in simulation [120]

Variable	$\dot{\varepsilon}_0$	A	B	C	n	m	α	D	E
Unit	1/s	MPa	MPa						
Value	2000	724.1	683.1	0.035	0.47	1	0	1	1

In the above equation, constants A, B, C, n, m are called as the yield stress coefficient, plastic strain coefficient, strain rate coefficient, hardening coefficient and thermal softening coefficient respectively. The friction model implemented in this model is simple shear friction model, which states that the friction force depends on the fraction of

equivalent shear stress, not on the normal force like the Coulomb friction model [37]. The friction in the interface zone is modeled using the Eq. (34) given below.

$$\tau = km \tag{34}$$

where, τ is friction force, k is equivalent shear stress and m is the shear friction factor. The selection of this friction model with friction factor, m=0.82 is based on several researches [124, 125, 137, 138] where this model has been validated comparing with the cutting forces, temperatures, and chip geometries. The thermal boundary conditions were applied for the heat losses from the tool or workpiece surfaces to the environment, and from the workpiece or chip surfaces to the cutting tool. The first process is affected by a convective coefficient (h_c) and the latter is affected by heat transfer coefficient or interface heat transfer coefficient (h). These can be explained mathematically as follows.

$$q = h_c (T_w - T_0) \tag{35}$$

$$q = h(T_w - T_t) \tag{36}$$

where h_c and h are convection coefficient and heat transfer coefficient respectively, T_w is workpiece or chip surface temperature, T_0 is the ambient temperature and T_t is the tool surface temperature during the cutting process. The complete method for the above modelling is presented as a flow chart (Appendix C).

5.3 Simulation Results and Discussions

To validate the numerical model, the model and experimental results for cutting forces and tool tip temperature were compared for both the cutting processes and discussed as follows.

5.3.1 Cutting force validation

A model can never be accepted until the results are validated with the experimental results. Validations for several runs were made comparing the numerical results with the measured results for the cutting forces during CT and UVAT as shown in Figures 5.3 (a) and (b). Good accuracy can be observed as the relative error percentages (R.E.) are low for

most of the runs with a highest value of 30.03% for the run number 91 during CT simulation. The relative error for both the models can be found out by following Eq. (37). The average error for CT and UVAT were calculated and found to be 9.50% and 6.80% respectively. The lower percentages of average errors depict that the models can be accepted to investigate the effect of process parameters predicting complex outputs occurring at the cutting zone.

$$\text{Relative Error (\%)} = \left| \frac{\text{Experimental Value - Simulation value}}{\text{Experimental value}} \right| \times 100 \tag{37}$$

Additionally, Figure 5.4 shows the comparative force history diagram for both the cutting processes for a single cycle after reaching steady state. On applying the ultrasonic vibration, the magnitude of average force was significantly reduced, almost 40% due to the intermittent motion of the cutting tool in the case of UVAT. The generated force was continuous and reached a steady state in case of CT process, due to continuous engagement of the insert with the workpiece. Inversely, in UVAT process, force reached to the maximum only when the insert was fully in contact with the workpiece and chip. Further, the transient and persistent phenomenon of force generation can be explained from the stress generations in different stages of the cycle (as in Figures 5.5 and 5.6), such as, during the first stage, the insert approaches towards the workpiece with an effective stress of 0.079 MPa. As the insert in contact with the workpiece during the penetration stage of the cycle, the stress increases up to 1820 MPa and reaches a maximum value of 2890 MPa nearly equal to the CT process. In the 3rd stage, unloading stage, the stress generation decreases from 2890 MPa, and ceases to 0.087 MPa during the withdrawal stage of the cycle. On the contrary, the stress generation was found to be a continuous process approx. 2800 MPa during CT process.

Figure 5.3 Comparison of main cutting forces with the measured results (a) CT (b) UVAT

Figure 5.7 (a)-(d) depict the effect of cutting velocity on the forces for both the cutting processes. Cutting velocity has a direct effect on the insert movement; as the increasing cutting velocity increases the tool engagement time resulting higher cutting forces and the effect of UVAT process ceases as the velocity reaches to the critical velocity of the cutting tip (with increase of TWCR).

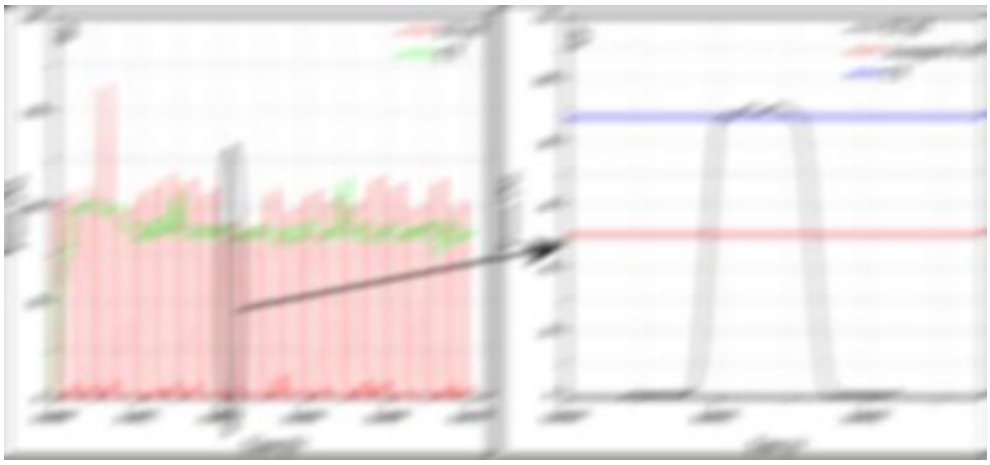

Figure 5.4 (a) Force generation from Deform 3D® for both CT and UVAT (b) single cycle of a UVAT simulation with reduction in average cutting force

Figure 5.5 Transient cutting in UVAT at V_c= 18m/min, s= 0.04mm/rev and d= 0.14 mm

Figure 5.6 Continuous cutting in CT at V_c= 18m/min, s= 0.04mm/rev and d= 0.14 mm

Figure 5.7 Effect of cutting velocity on the main cutting force obtained from both experiment and simulation for CT and UVAT at (a) s= 0.04 mm/rev, d= 0.14 mm (b) s= 0.08 mm/rev, d= 0.18 mm (c) s= 0.08 mm/rev, d= 0.26 mm (d) s= 0.08 mm/rev, d= 0.26 mm

5.3.2 Tool temperature validation

For several experimental runs, simulations were carried out to analyze the thermal phenomena occurred in the cutting zone and tool temperature evolution as well. To achieve the steady state temperature, a global heat transfer coefficient (h= 1000 kW/m$^{2\,0}$C [124, 137]) was carefully chosen. Figure 5.8 depicts the tool tip temperature evolution for different heat transfer coefficient, h with a temperature convergence for h=1000 kW/m^{2} ^{0}C.

Figure 5.8 Tool tip temperature evolution with different values of h (in kW/m$^{2\,0}$C)

The steady state tool temperatures obtained from both experimental and simulations were compared with a maximum error percentage of 30.95% for the 28th run. Figures 5.9 (a) and (b) depict a comparative case for the tool temperature evolution for both the processes. It shows that the simulation results provide quite satisfactory and supported results for the measured temperature evolution during both the cutting processes making a good correlation with the experiment. Further, the average relative error for both the CT model and UVAT results were found to be 8.08% and 9.19% respectively.

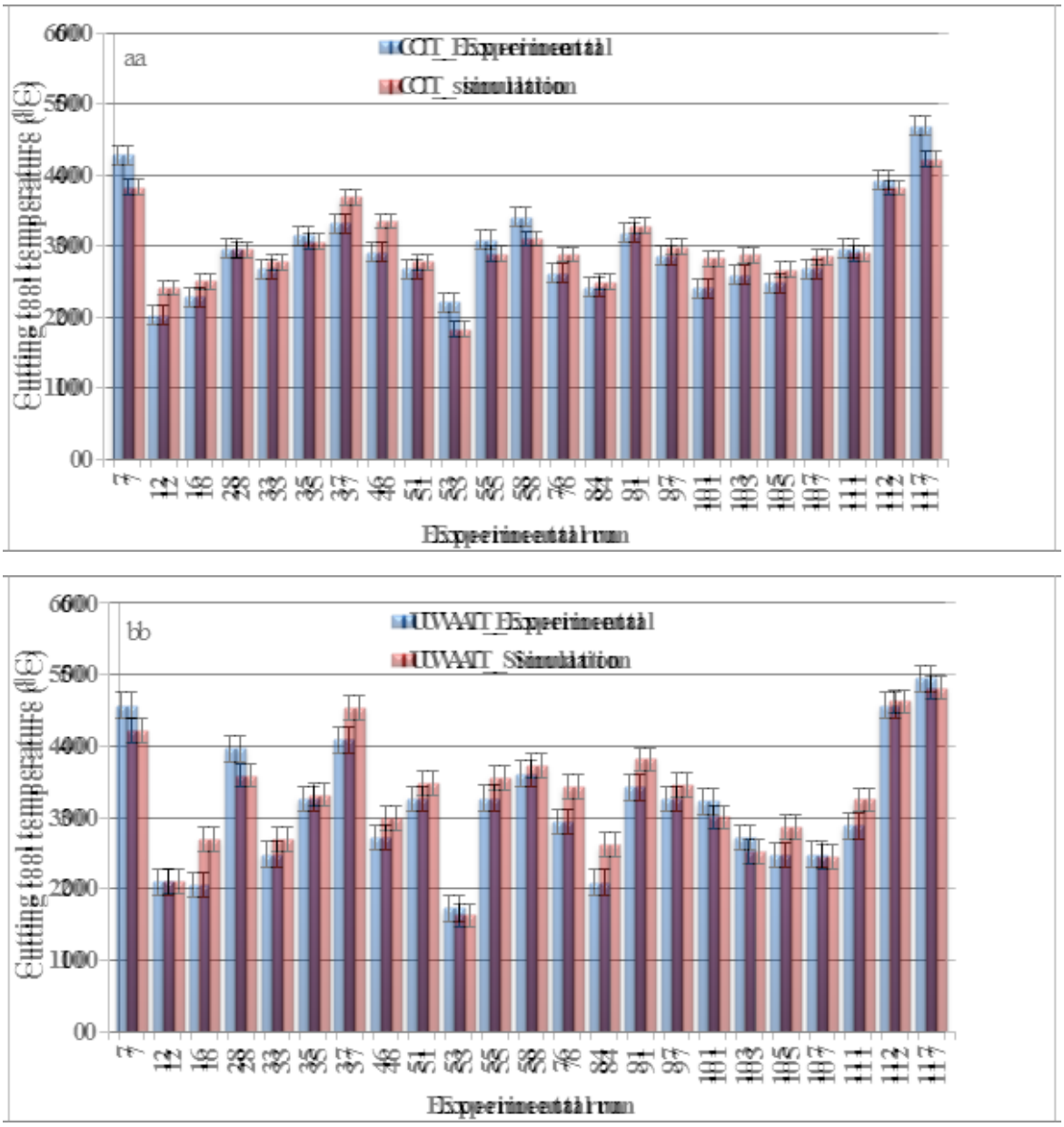

Figure 5.9 Comparison of simulation results for cutting tool temperature with the measured results (a) CT (b) UVAT

Steady state temperature was obtained approximately after 0.0003 seconds for several simulations with h=1000 kW/m^2 ^{0}C. Figure 5.10 shows the measured and simulated results for tool tip during both the machining processes. The temperature evolution characteristics during the UVAT process is oscillating type as due to the intermittent motion of the cutting insert. During the contact stage, the temperature increases to the maximum value and cools down during the withdrawal stage, unlike the CT process in which, the temperature remains steady along with the cutting process due to continuous engagement of the tool with the workpiece.

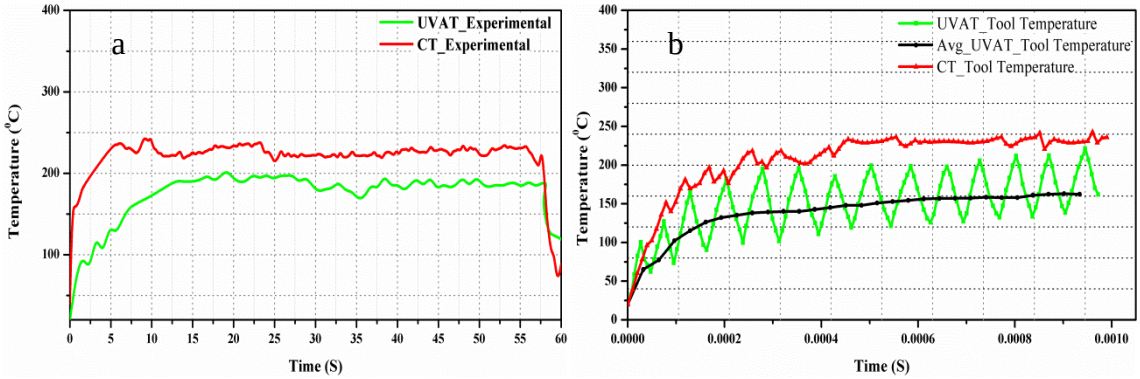

Figure 5.10 Steady state tool during (18 m/min, f=0.04 mm/rev, d=0.14 mm) (a) Measured temperature (b) Point tracking result from the FE simulation

Comparing the UVAT simulations results with that of CT, the tool temperature got reductions like 10.77 %, 12.77 %, and 12.04 % for the run no 53, 12, and 103 respectively with the cutting velocity of 18m/min, 30 m/min and 40m/min. The possible reasons could be the aerodynamic lubrication that reduces the heat propagation to the tool during the separation period due to the intermittent motion of the tool. Also, at the same velocity having the maximum feed and depth of cut value, the UVAT temperature exceeds the CT temperature. It implies that not only the lower cutting velocities but also lower feed rates and depth of cuts are suitable for the UVAT process as far as temperature evolution is concerned. Further, the tool temperature during UVAT processes inclined towards the CT temperatures as the speed increases to 30 m/min and surpassed by several percentages as the velocity reached to 40m/min as shown in Figure 5.11. This can be explained with the help of UVAT process mechanism; as the cutting velocity increases, the separation time between the tool and workpiece reduces since the cutting velocity approaches towards the critical velocity and the effect of additional energy supplied by the ultrasonic vibration explained by several researchers. Furthermore, the finite element models can predict the interface temperature that could not be measured during our experiment. The temperature distribution obtained from the FE model are depicted in Figures 5.12 (a)-(f) with the temperature characteristics.

Figure 5.12 Interface temperature with the average value and temperature distributions for (a, d) 18 m/min (b, e) 30 m/min and (c, f) 40 m/min

Primarily, the temperature distribution on the tool tip surface during the cutting process affects the tool life and the predicted temperature distribution for both the processes are shown in Figure 5.13. It explains the tool temperature distribution during UVAT process drastically reduces due to the vibratory motion of the cutting tool which could directly affect the tool life in a better way making this process better compared to the CT process.

Figure 5.13 Temperature distributions on the tool surface from the cutting tip (after reaching steady state)

5.4 Conclusions

In the present chapter, a 3D thermo-mechanical model was prepared for both the cutting processes considering non-linear material flow stress and a suitable friction model with a proper global heat transfer coefficient. The following conclusions can be drawn from the above observations:

(i) The cutting force increased with cutting velocity due to the escalation of contact period of the tool with the workpiece at a higher velocity. For principal cutting force, the average relative errors were found to be 9.50% and 6.80% for CT and UVAT respectively.

(ii) The steady state temperature during the cutting processes has been investigated by selecting a suitable friction model with global heat transfer coefficient, h=1000kW/m^2 ^{0}C. Tool temperature results have been validated with the experimental results with the average relative error percentages of 8.08% and 9.19% for CT and UVAT respectively. Further, it has been noted that the temperature distribution on the tool surface is comparatively lower than tool temperature distribution during CT process.

(iii) UVAT process does not necessarily reduce the tool temperature always; rather the evolution of cutting temperature majorly depends on the cutting velocity, feed rate, and depth of cut. For instance, at a minimum cutting velocity with minimum feed and depth of cut, the tool temperature during UVAT was found to be lower than that of CT temperature. But, it surpassed the temperature for

CT, when UVAT was carried out with high feed rate and depth of cut. Therefore, low cutting velocity, feed, and depth of cut were favorable to UVAT process.

(iv) Finally, the interface cutting temperature was predicted from the model after the validation of the model and the same found to be increasing with the increase in cutting velocity.

Chapter 6

Chip Morphology, Tool Wear, and Surface Integrity Investigations

Titanium alloy, Ti-6Al-4V shows serious machining challenges due to inherent characteristics like high hardness at elevated temperature, high affinity towards the cutting tools and reduced thermal conductivity that demands novel machining processes to cut these “hard to cut” alloys. Ultrasonic vibration assisted turning is one of the novel machining process to enhance the machinability of “hard to cut” alloys. In a machining process, surface finish, tool life, and chip morphology are the basic characteristics that rate the machinability of material for a particular material removal process. The present chapter focuses on the investigation of machinability indices like chip morphology, surface integrity, and tool wear with a comparative study applied to Ti-6Al-4V using CT and UVAT processes.

6.1 Chip Morphology

The quality of machining and the degree of ease in cutting can be studied from the nature of chip produced during a cutting process [139]. Further, the nature of chip affects the tool workpiece interaction influencing the tool life. Chip morphology includes chip reduction ratio, chip thickness, equivalent chip thickness, and segmentation frequency of the chips. It is observed that during both the cutting operations, the chips formed were serrated or saw tooth type. Different terms related to chip morphology are peak height (h_{max}), valley height (h_{min}), pitch of the tooth (P_c), saw tool angle (Φ_s) shown in Figure 6.1.

It was observed that thicknesses of the chip produced during UVAT were thinner than that of CT process. Further, the UVAT chips were smooth, more curled, and uniform, unlike CT chips. The chip thickness during CT was thicker due to the continuous contact of the tool tip with the workpiece, whereas, the chip formed during UVAT was thinned due to intermittent contact of the tool with the workpiece. Figure 6.2 shows a comparative study of chip thickness at different cutting velocities keeping feed, s at 0.08 mm/rev and depth of cut, d at 0.26 mm. It is evident that chip thickness decreases with the increase of cutting velocity. The reduction in chip thickness correlates with the cutting force reduction

with the increase in velocity. Similar results were observed by researchers, Li and shih [114]. It is also observed that the difference between the chip thickness obtained by CT and UVAT decreases with increase of cutting velocity. It is due to the fact that as cutting velocity increases, the velocity difference (Between the cutting velocity and tool tip velocity) decreases, and the UVAT approaches the CT process. Similarly, the chip reduction coefficient was calculated dividing the chip thickness with the uncut chip thickness and shown in Figure 6.3.

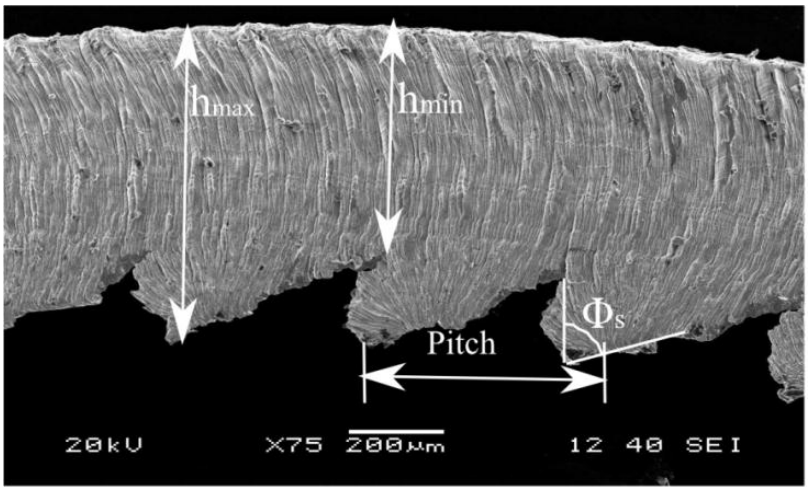

Figure 6.1 Saw tooth type chip with different terms related to chip

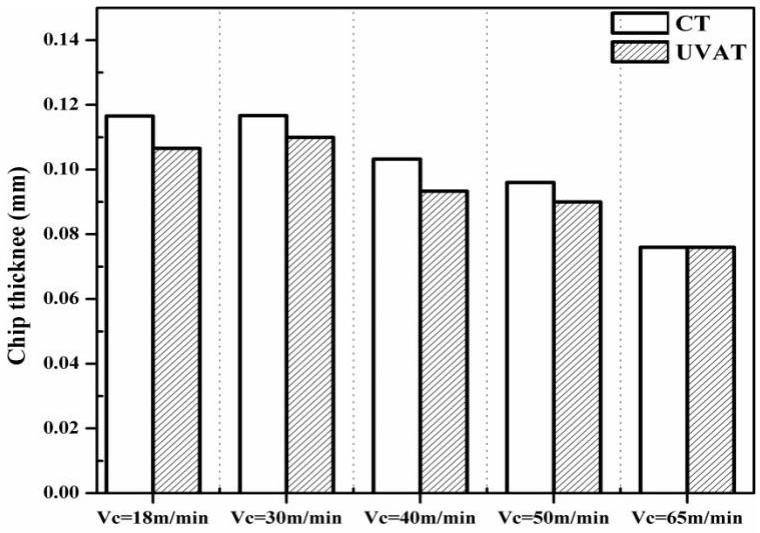

Figure 6.2 Comparison of chip thickness at different cutting velocity for CT and UVAT at constant feed, s= 0.08 mm/rev, and depth of cut, d= 0.26mm

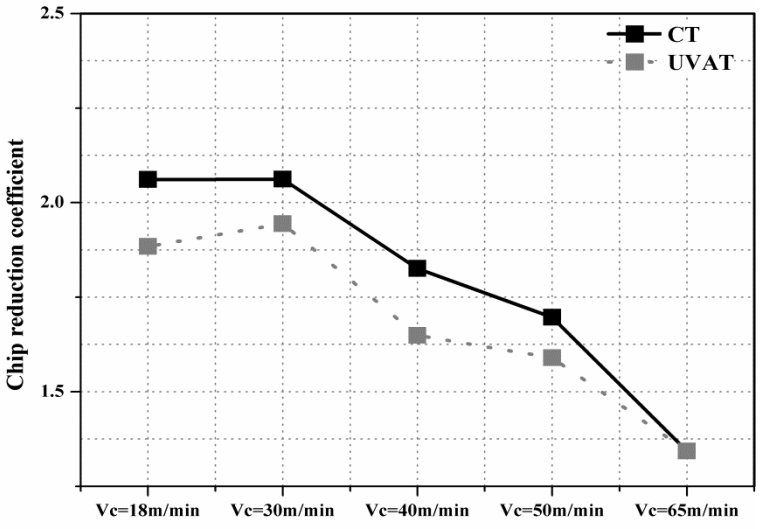

Figure 6.3 Comparison of chip reduction coefficients at different cutting velocities for CT and UVAT at constant feed, s= 0.08 and depth of cut, d= 0.26mm

In order to get a better understanding of the chip morphology, the pitch of serration, P_c and segmentation frequency of chips were calculated for both the cutting processes. Initially, the chips were observed under the scanning electron microscope and later, measured using ImageJ®. Figure 6.4 shows the serrated types of chips generated during CT and UVAT at different cutting conditions where the segmentation frequency can be calculated using following equation:

$$Segmentation\ frequency\ of\ chip,\ f_{cs} = \frac{V_c}{P_c} \tag{38}$$

Where, V_c is the cutting velocity in mm/sec, P_c is the pitch of the tooth generated in the serrated chips and f_{cs} is the segmentation frequency in Hz. Figure 6.5 shows the segmentation frequency of the chips. It is evident from the result that the frequency values were significantly higher in the case of chips produced during UVAT. The prime reason is combined effect of cutting velocity and additional energy supplied by the ultrasonic vibration that increases the relative velocity that generates the high strain rate and thermal softening at the process zone during UVAT compared to CT.

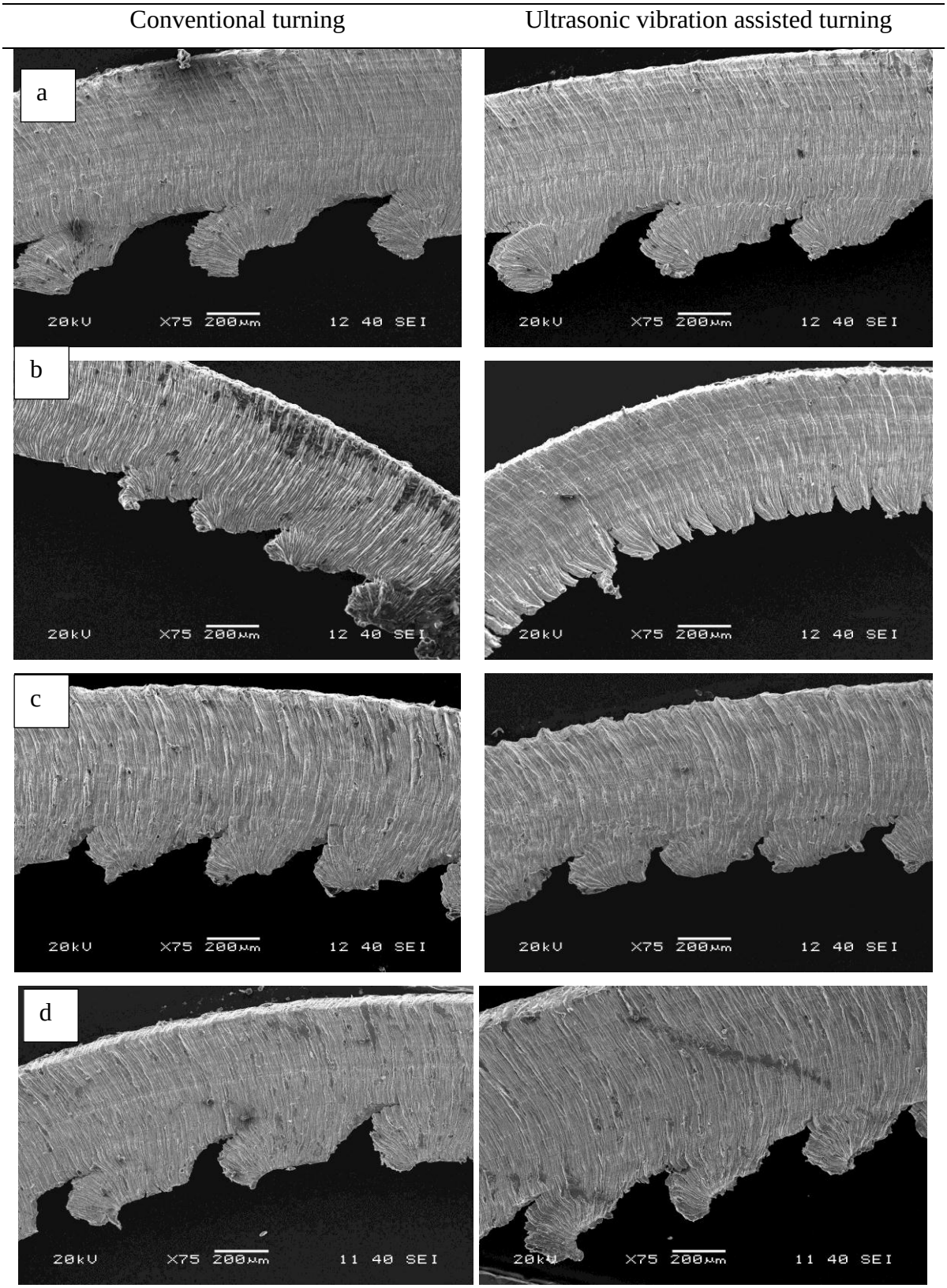

Figure 6.4 Comparison of chip geometry generated during CT and UVAT (a) Vc= 30 m/min, s= 0.08 mm/rev, d= 0.26mm (b) Vc= 40 m/min, s= 0.08 mm/rev, d= 0.26mm (d) Vc= 50 m/min, s= 0.08 mm/rev, d= 0.26mm (d) Vc= 65 m/min, s= 0.08 mm/rev, d= 0.26mm

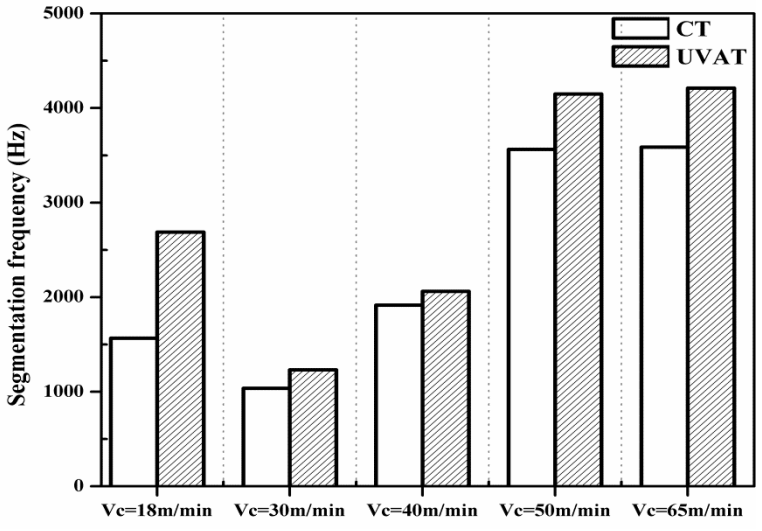

Figure 6.5 Comparison of segmentation frequency at different cutting velocity for CT and UVAT at constant feed, s=0.08 mm/rev, and depth of cut, d= 0.26mm

6.2 Tool Wear

Tool wear is an important parameter that affects the machined surface quality and economics of any machining process. In the present investigations, the cutting insert was observed for both flank and crater wear, but the first type was more prevalent during both the cutting processes. Figure 6.6 shows the optical microscope images of the flank wear measured after two mins of intervals for each run with a total duration of 10 mins. It depicts that the flank wear increases with the machining time and cutting velocity. At low cutting velocity during UVAT, the flank wear growth was tolerable, but substantial growth was noted at higher cutting velocity for both the cutting processes. Additionally, there were formations of buildup edges during CT process (after six mins at different velocities), which was not observed during UVAT due to the intermittent nature of tool that prevents sticking of workpiece or chip onto the tool face improving the surface quality. The generation of buildup edges during CT of Ti-6Al-4V could be a reason for poor machined surface. The above explanations can be described graphically in Figure 6.7 by measuring average flank wears using ImageJ® software at different machining times varying the cutting velocities. Finally, the wear evaluations after ten mins of cutting during CT and UVAT were observed under scanning electron microscope and shown in Figure 6.8 (a, b).and (c, d). The cutting edge used for the CT process was with a fracture near to the cutting edge, and also with flank wear whereas the insert used for UVAT process was only with the flank wear. The increase in the average surface roughness value could be due to the fracture occurred during the CT process (Described in Chapter 4)

which was not in the case of UVAT process. Further, the failure in the cutting edge causes the increase in magnitude of force for CT process which is not prominent in the UVAT. Similar observations were made by several researchers concluding the aerodynamics lubrication as the major reason for better tool life during UVAT process at lower speed [34, 70, 82].

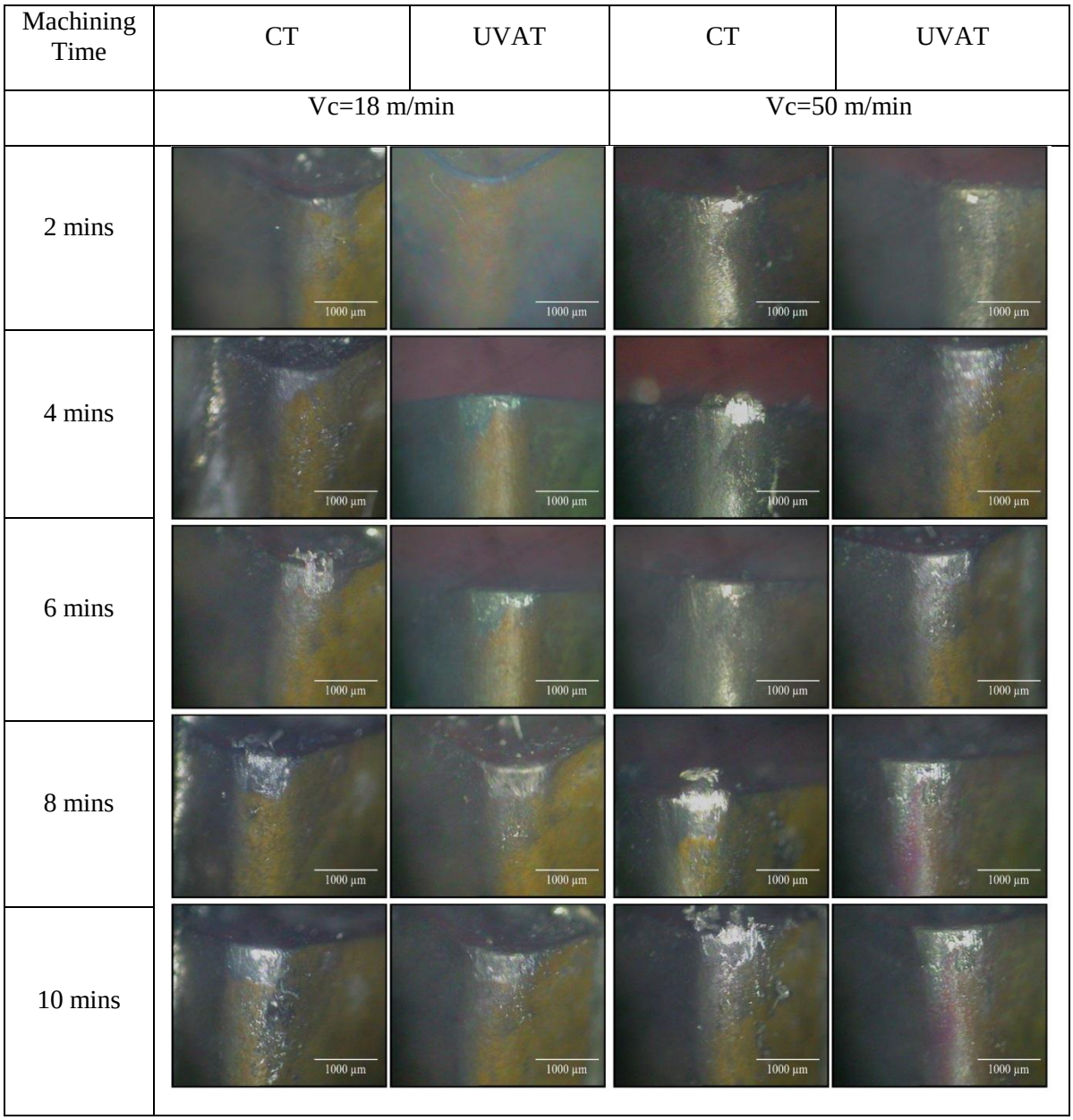

Figure 6.6 Flank wear evolution during CT and UVAT at different velocities varying machining period at constant feed, s= 0.04 mm/rev and depth of cut, d= 0.14mm

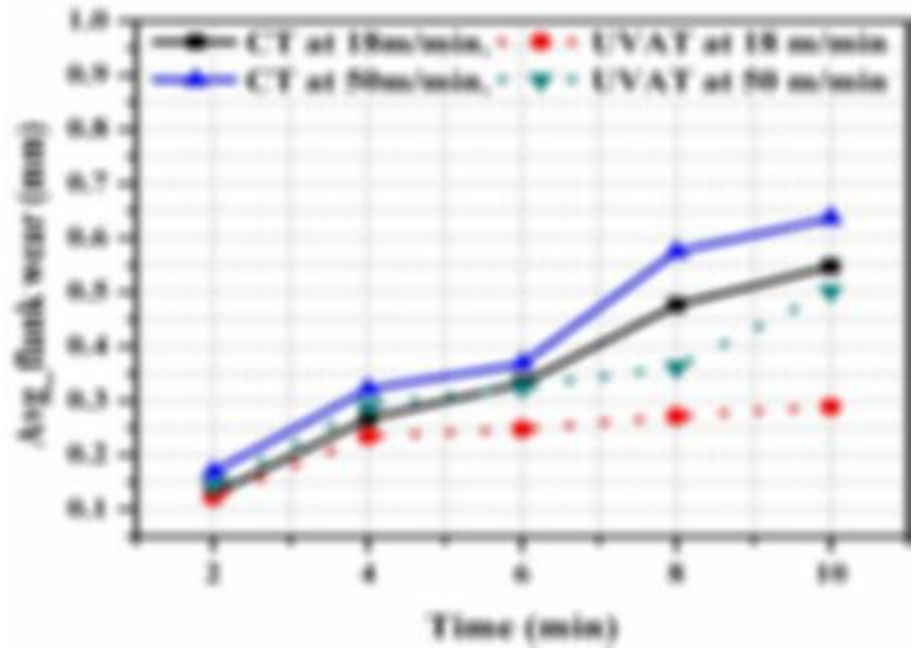

Figure 6.7 Average flank wear evolution during CT and UVAT at different velocities varying machining period at constant feed, s= 0.04 mm/rev and depth of cut, d= 0.14mm

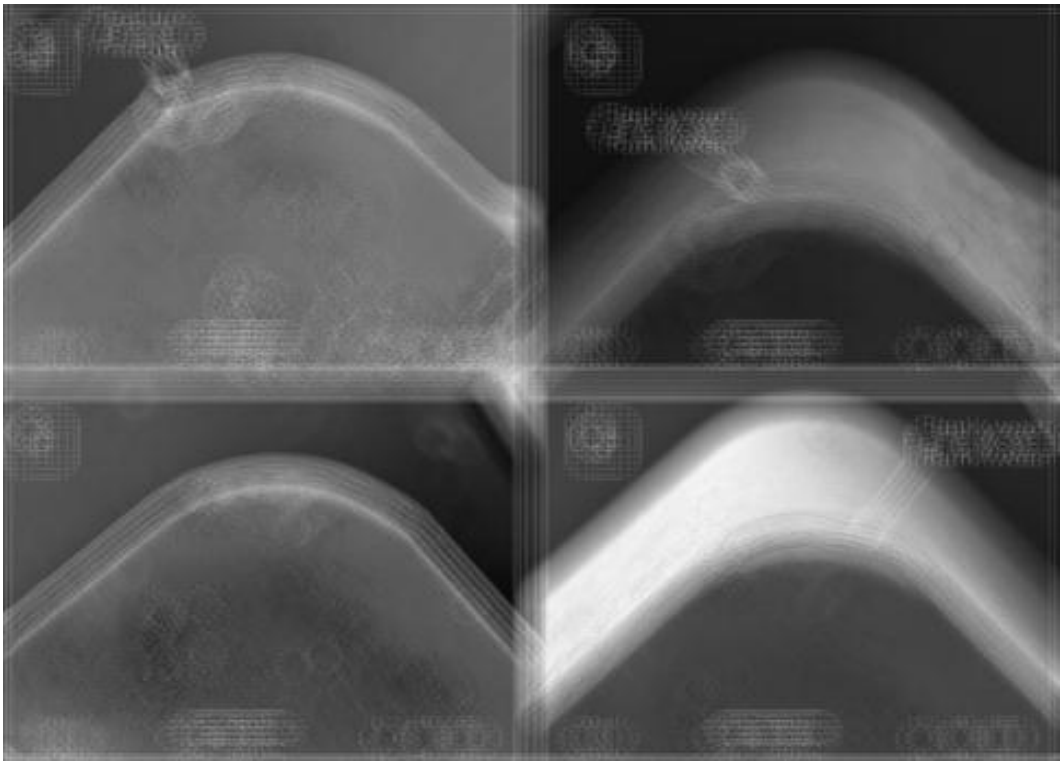

Figure 6.8 SEM image of tool wear at V_c= 18 m/min, s= 0.04 mm/rev, d= 0.14mm for (a,b) CT process and (c,d) UVAT process.

6.3 Surface Integrity

Surface finish is an important output in the production engineering that affects directly on the fatigue life for the most material and influences the finishing cost [31, 90, 140]. The obtained surface finishes for both the processes were measured with the help of Handysurf® and the machined surfaces were investigated under scanning electron microscope (SEM) as depicted in Figure 6.9. The CT machined surface contained several scratches along with the debris and accumulated materials, that were absent in the later surface, with a Ra value of 1.5 µm. Similar surface pattern of the surface was noticed by several researchers during the CT process of titanium alloys [49, 141]. However, the UVAT machined surface showed an improved surface quality with a R_a value of 0.9 µm with a reduction of 40 %. The observation confirms that the UVAT process can be thought a better machining procedure with limited and low cutting speed range as suggested by several researchers appeared to Ti-6Al-4V.

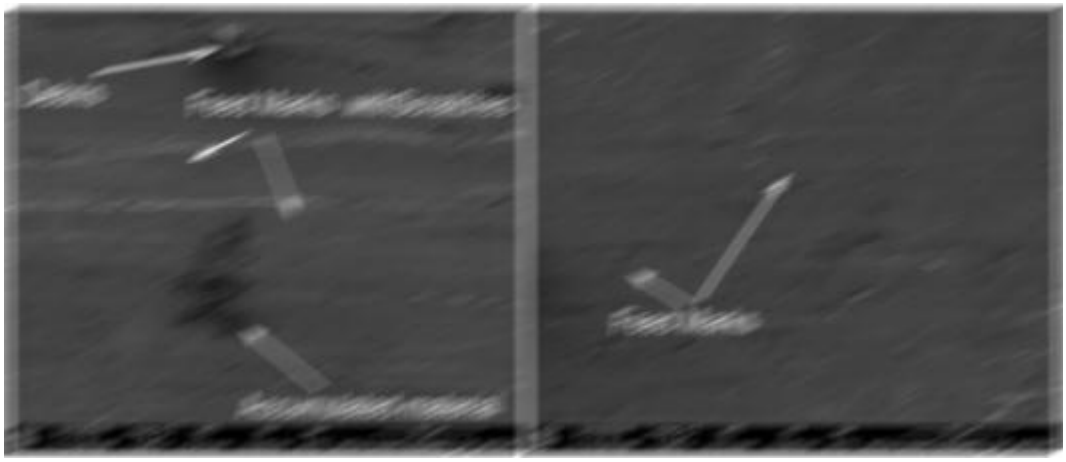

Figure 6.9 SEM images of both the machined surfaces (a) CT machined, and (b) UVAT machined surface

6.4 Effect of Lubrication

The effect of coolant under wet cutting on the machinability of Ti-6Al-4V during both the cutting conditions was investigated. Wet cuttings were carried out using coolant prepared from soluble oil (base oil and emulsifying agent, Veedol Solucut®) mixed with water in the ratio of 1:10. The machining was carried out for cutting condition, Vc= 18 m/min, s= 0.04 mm/rev and d= 0.14 mm with a fixed flow rate of 0.68 lpm. There were significant reductions in cutting forces during turning of Ti-6Al-4V for both the processes, for

instance, almost 23% and 12% of reductions were noted for CT and UVAT respectively. The reason could be the reduction in the friction coefficient at the contact zone due to physical lubricity. Additionally, the chip formed with the use of coolant is more curled and continuous (Figure 6.10). The surface roughness values were drastically reduced with a value of 1.16 µm and 0.53 µm for CT and UVAT machined surfaces with reductions of 22.67 % and 41.11 %. Therefore, use of a lubricant can be additional assistance to enhance the machinability of Ti-6Al-4V.

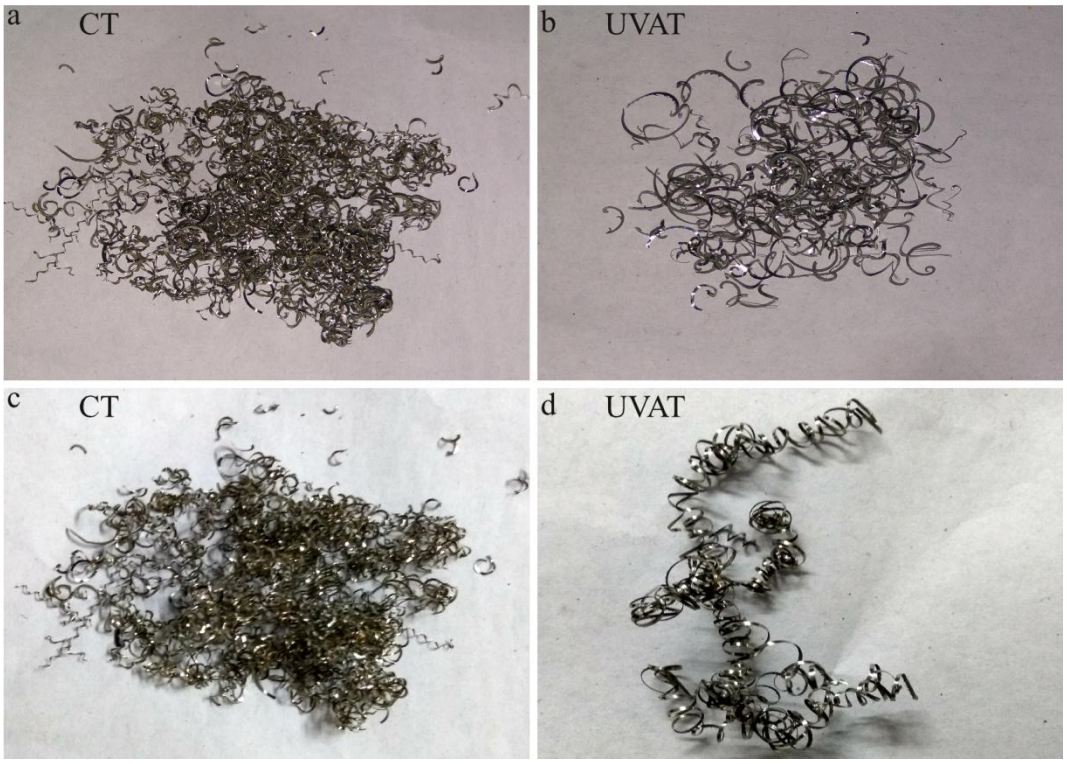

Figure 6.10 Chip formed during CT and UVAT (a, b) with dry cutting (c, d) with wet cutting

6.5 Conclusions

The following conclusions can be drawn from the chip morphology, tool wear, and surface integrity investigations:

(i) The chip formed during UVAT was comparatively thinner than the chip formed during CT due to intermittent contact of the tool with the workpiece during UVAT.

(ii) The chip reduction coefficient during UVAT were found to be low compared to the CT process, explains the reduction in the cutting forces during UVAT

than the latter case. Further, the chip reduction coefficient decreased due to increase in cutting velocity.

(iii) UVAT generated chips had higher segmentation frequency than the CT, depicts that during UVAT high strain rate and thermal softening occur at the cutting zone enhancing the material removal rate.

(iv) UVAT enhanced the machinability of Ti-6Al-4V reducing the tool wear to a great extent. During CT, fracture with flank wear was observed due to continuous contact of the tool with the workpiece.

(v) UVAT produced an improved machined surface, unlike CT machined surface with 40% reduction in average surface roughness. Further, the CT machined surface was having surface errors like debris, scratches and accumulated material with feed marks. In UVAT machined surface, feed marks were not prominent with enhanced the surface finish.

(vi) The use of lubrication was effective for both the processes reducing cutting forces by 23% and 12% for CT and UVAT respectively. Additionally, the lubricity helped generate an improved machined surface reducing the roughness magnitude by 22.67 % and 41.11 % for CT and UVAT respectively.

Chapter 7

Conclusions

The present research focuses on the investigation of turning machinability of titanium alloy, Ti-6Al-4V during conventional turning and ultrasonic vibration assisted turning. Further, the turning operations were simulated using finite element model using Deform3D® to investigate the effect of controlling parameters on the output responses like cutting force, surface roughness, and tool temperature. Finally, machinability indices like chip morphology, surface integrity, and tool wear were investigated. The following observations can be drawn from the above research work.

7.1 Major Findings

The present chapter includes all the major findings obtained from the above chapters investigating the acoustic horn, experimental and numerical studies of CT and UVAT of Ti-6Al-4V. The findings can be summarized as follows:

- Unlike a conventional design of horn i.e. uniform horn design, a flexible type has been proposed and analyzed using finite element method. The resonant horn length was found out from the analytical method corresponding to the operating ultrasonic frequency, 20 kHz ± 500 Hz and compared with the experimental results. The horn length for single uniform stepped horn, and flexible horn were found to be 125.5mm and 125mm with error percentages of 1.19 % and 3.40 % respectively on comparing with the analytical length.
- Dynamic analysis results confirm an allowable stress concentration range for different stresses during the cyclic loading that is below the fatigue strength (269 MPa) of the proposed horn material. Additionally, the maximum stress is observed at the nodal points.
- Further, both theoretical and analytical amplification ratios were compared. The errors of 1.68% and 2.33% are found for conventional stepped horn and flexible horn respectively. It substantiates that finite element method is a powerful tool to

model and analyse the prototype before the actual fabrication, which is cost saving and economical.

- Experimental investigation of both CT and UVAT processes depicted that on applying ultrasonic vibration to the cutting tool, there were significant reductions (40.07%, 34.77%, 23.57%, 14.09%, and 5.06% at V_c= 18min to 65 m/min) in principal cutting forces comparing with the results obtained during the CT.

- The UVAT was found to be a novel technique improving the machined surface while comparing with the results obtained from the CT process. Almost, 41% of the reduction in average surface roughness was observed during UVAT process compared to the CT process with a constant velocity of 18m/min varying the depth of cuts from 0.14 mm to 0.30 mm for different feed rates.

- For CT and UVAT operations, the R- Squared and adj. R- Squared values were found to be above 90% showing the reliability and precision during the experimental investigations. Similar observations were found for average surface roughness and tool temperature.

- A 3D thermo-mechanical model was prepared for both the cutting processes and the model was validated comparing the main cutting force results with the experimental results. For principal cutting force, the average relative errors were found to be 9.50% and 6.80% for CT and UVAT respectively.

- The steady state temperature during the cutting processes has been investigated by selecting a suitable friction model with global heat transfer coefficient, h=1000 $kW/m^2\ ^0C$. Tool temperature results have been validated with the experimental results with the average relative error percentages of 8.05% and 9.15% for CT and UVAT respectively.

- Finally, the interface cutting temperature was predicted from the model after the validation of the model and found to be increased with the increase in cutting velocity.
- UVAT produces an improved machined surface, unlike CT machined surface with 41% reduction in average surface roughness. Further, the CT machined surface was having surface errors like debris, scratches and accumulated material with feed marks. The chip reduction coefficients during UVAT were found to be low

compared to the CT process, explains the reduction in the cutting forces during UVAT than the latter case. Further, the chip reduction coefficient decreased due to increase in cutting velocity.

- The use of coolant for both the processes was found to be effective in a positive manner enhancing the machinability of titanium alloy, Ti-6Al-4V. Significant reductions in forces and surface roughness were noted during wet cutting, such as 23% and 12% reductions in cutting forces, and 22.67 % and 41.11 % reductions in average roughness were observed for CT and UVAT respectively.

7.2 Conclusions

From the above major findings, following knowledge enhancements and final conclusions can be drawn:

- A flexible acoustic stepped type horn has been proposed and numerically analyzed using finite element method to get the resonant horn length and amplification factor. The analysis has been done by modal and harmonic analysis.
- Based on the numerical analysis, acoustic horn has been fabricated and designed. Numerically obtained length has been found very close to that of the fabricated and tuned one. It indicates that finite element method is a powerful tool to predict and optimize the design of a product.
- Experimental investigation of CT and UVAT of Ti-6Al-4V depicts that significant reduction in cutting forces has been noted during UVAT process due to the intermittent characteristics of the cutting tool. Unlike CT in which the cutting tool is in continuous contact with the workpiece, UVAT process has been found to improve the machined surface.
- Lower cutting velocities combined with the minimum value of the depth of cut and feed rates were found to be best suited cutting conditions to carry out the UVAT process of Ti-6Al-4V as far as temperature evolution is concerned.
- A 3D finite element model has been modelled for both the cutting processes applied to Ti-6Al-4V and found to be resourceful in studying the effect of cutting parameters on the output responses. Further, the experimental validations of FE results depict that the present models are reliable.

- Finally, the observations of the machinability indices like chip morphology, surface integrity, and tool wear have confirmed the suitability of UVAT process for Ti-6Al-4V to get enhanced machined surface. Thin and smooth chip formations with enhanced machined surface were observed during UVAT making it a superior and novel machining method.
- The use of lubricant during both the processes affected the machinability in a positive manner reducing cutting forces and surface roughness. Therefore, coolant can be an additional assistance to enhance the machinability of Ti-6Al-4V using UVAT process.

7.3 Scope of Future Works

The present work provides a wide scope for future study to explore various aspects of UVAT process. A few scopes have been depicted for research works as follows:

- Heating of the acoustic horn has been a major problem in an ultrasonic system. Therefore, a novel design to prevent the heating issue can be further studied.
- Effect of tool geometries like rake angle, nose radius, etc., and tool coatings on the UVAT process can be studied for extended works.
- Investigations of UVAT with different cooling methods using emulsified coolants, minimum quality lubrication (MQL), and cryogenic coolants can be assessed.
- Oblique cutting using UVAT and its effect on the output responses can be researched to explore more in UVAT method.

Appendices

Appendix A: Experimental results

The following experimental results were obtained during CT and UVAT.

Appendix B: Statistical formulations

ANOVA Test

ANOVA test is used to analyze the variations among two or more means. It is derived from a partitioning of total variability into parts. The total corrected sum of square can be written as follows,

$$\text{Total Sum of squares } (SS_T) = SS_T = \sum_{i=1}^{a}\sum_{j=1}^{n}\left(y_{ij} - \overline{y_{\bullet\bullet}}\right)^2 \tag{B.1}$$

Where, y_{ij} is the j^{th} observation taken under factor i^{th} level and $\overline{y_{\bullet\bullet}}$ is the average of total 'n' observations. Further, the sum of squares can be written as the addition of sum of the square of the treatment ($SS_{Teatment}$) and the sum of squares of the error (SS_E) as shown in Eq. (B.2).

$$\text{Total Sum of squares } (SS_T) = SS_T = \sum_{i=1}^{a}\sum_{j=1}^{n}\left(y_{ij} - \overline{y_{\bullet\bullet}}\right)^2 = SS_{Treatment} + SS_E \tag{B.2}$$

Where, $SS_{Treatment} = n\sum_{i=1}^{a}\left(\overline{y_{i\bullet}} - \overline{y_{\bullet\bullet}}\right)^2$ and $SS_E = \sum_{i=1}^{a}\sum_{j=1}^{n}\left(\overline{y_{ij}} - \overline{y_{i\bullet}}\right)^2$, $\overline{y_{i\bullet}}$ is the average of all the measured data under i^{th} treatment.

Degree of freedom (DOF) depicts the number of independent variables that are free to vary. It can be found out by the following formula.

$$Total\ \deg ree\ of\ \ freedom = n - 1 \tag{B.3}$$

Where, n is the total number of observations.

Mean square value can be calculated as the ratio of the sum of square to the degree of freedom as shown in Eq. (B.4). It describes an estimate of population variance.

$$Mean\ Square = \frac{Sum\ of\ \ square}{\deg ree\ of\ \ freedom} \tag{B.4}$$

Similarly, the mean square for treatments and error can be calculated accordingly shown in Eq. (B.5) and (B.6).

$$MS_{Treatment} = \frac{SS_{Treatment}}{a-1} \tag{B.5}$$

$$MS_{E} = \frac{SS_{E}}{N-1} \tag{B.6}$$

Where, $MS_{Treatment}$ and MS_{E} are mean square error for treatment and error respectively. (a-1) and (N-1) are the degree of freedom of treatments and errors.

F- Statistics depicts the ratio of mean squares. It can be calculated as the ratio of the mean square of a term to the mean square of the error and can be written as follows. Additionally, the effect of variables on the output and their interactions can be known from the F- value.

$$F = \frac{MS}{MS_{E}} \tag{B.7}$$

p-Value depicts the significance of the difference in the means between the groups. Usually, if the p-value is less than the 0.05, then the differences between some of the means are significant and when the value is greater than 0.05, the differences are not significant. The model adequacy was checked by R- Squared and adjusted R- squared value and can be obtained from the following formula. The R-square value indicates the percentage of the variation in the output responses explained by the controlled input parameters. The larger magnitude of R-Squared value increases the degree of model acceptance.

$$R^2 = \frac{SS_{\mathrm{Re}gresion}}{SS_{Total}}$$

$$\text{or, } R^2 = 1 - \frac{SS_{Error}}{SS_{Total}} \tag{B.8}$$

From the above expression, it is evident that the addition of extra variables can increase the R-Square value whether the variables may or may not have a significant effect on the response. Therefore, one should not accept a model only by considering the higher magnitude of R-Squared value. To avoid the issue, adjusted R- Squared value is calculated and can be formulated using the Eq. (B.9).

$$adj\ R^2 = 1 - \frac{\frac{SS_{Error}}{n-p}}{\frac{SS_{Total}}{n-1}} = 1 - \left(\frac{n-1}{n-p}\right)\frac{SS_{Error}}{SS_{Total}} = 1 - \left(\frac{n-1}{n-p}\right)\left(1-R^2\right) \quad \text{(B.9)}$$

Where, n is the total sample size or observations, p is the number of independent variables. From the above Eq. (B.9), it is evident that increase in variables which do not have significant correlation with the output decreases the adjusted R-Squared value.

Appendix C: Flow chart for numerical model

The complete flow chart for model preparation of both CT and UVAT using finite element method is shown in the Figure C.1.

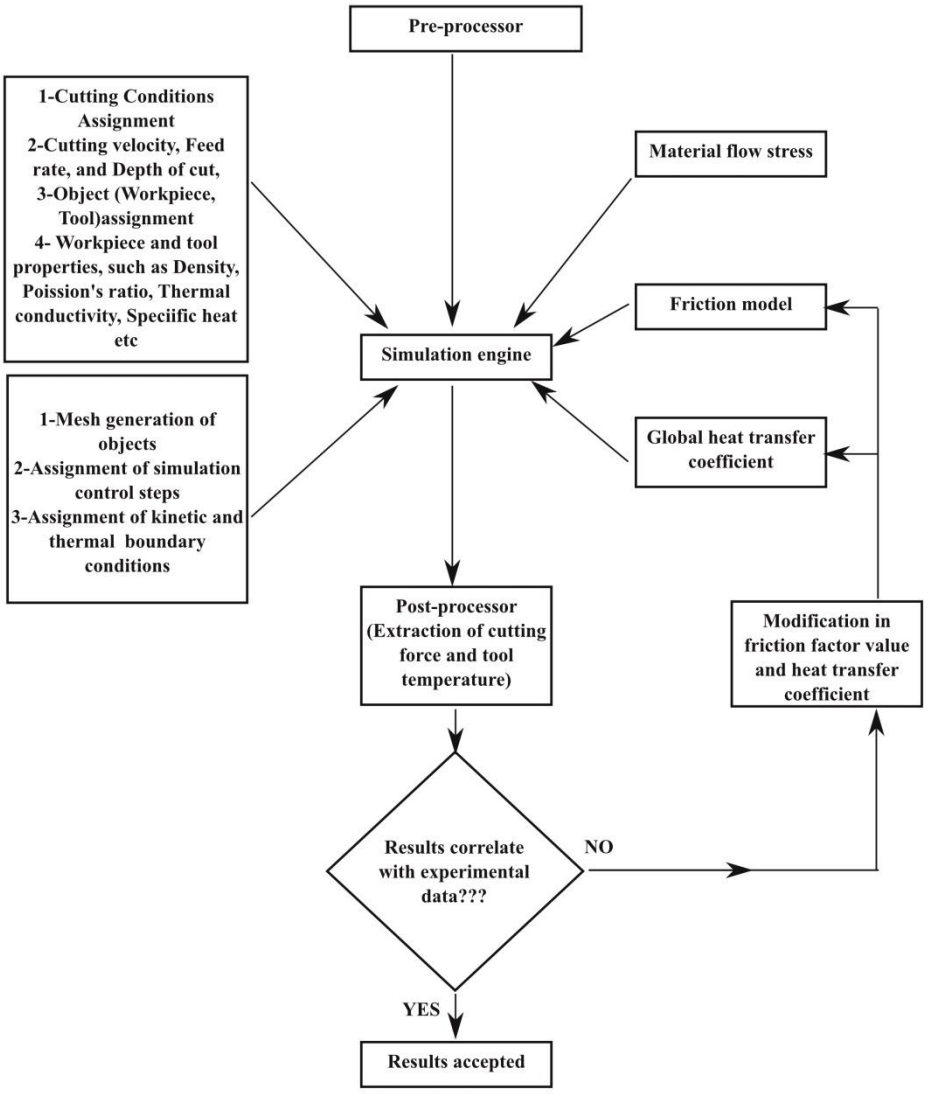

Figure C.1 Flow chart for numerical model preparation for CT and UVAT

References

[1] G. Welsch, R. Boyer, and E. Collings, *Materials properties handbook: titanium alloys*: ASM international, 1993.

[2] A. Machado and J. Wallbank, "Machining of titanium and its alloys—a review," *Proceedings of the Institution of Mechanical Engineers, Part B: Journal of Engineering Manufacture,* vol. 204, pp. 53-60, 1990.

[3] M. J. Donachie, *Titanium: a technical guide*: ASM international, 2000.

[4] B. Hanson, "Present and future uses of titanium in engineering," *Materials & Design,* vol. 7, pp. 301-307, 1986.

[5] S. R. Seagle, "The state of the USA titanium industry in 1995," *Materials Science and Engineering: A,* vol. 213, pp. 1-7, 1996.

[6] R. Boyer, "An overview on the use of titanium in the aerospace industry," *Materials Science and Engineering: A,* vol. 213, pp. 103-114, 1996.

[7] E. Ezugwu and Z. Wang, "Titanium alloys and their machinability—a review," *Journal of materials processing technology,* vol. 68, pp. 262-274, 1997.

[8] A. Hosseini and H. A. Kishawy, "Cutting tool materials and tool wear," in *Machining of Titanium Alloys*, ed: Springer, 2014, pp. 31-56.

[9] X. Yang and C. Richard Liu, "Machining titanium and its alloys," *Machining Science and Technology,* vol. 3, pp. 107-139, 1999.

[10] M. Baili, V. Wagner, G. Dessein, J. Sallaberry, and D. Lallement, "An experimental investigation of hot machining with induction to improve Ti-5553 machinability," in *Applied mechanics and Materials*, 2011, pp. 67-76.

[11] D. Thakur, B. Ramamoorthy, and L. Vijayaraghavan, "Study on the machinability characteristics of superalloy Inconel 718 during high speed turning," *Materials & Design,* vol. 30, pp. 1718-1725, 2009.

[12] K. Venugopal, S. Paul, and A. Chattopadhyay, "Tool wear in cryogenic turning of Ti-6Al-4V alloy," *Cryogenics,* vol. 47, pp. 12-18, 2007.

[13] R. Singh and J. Khamba, "Ultrasonic machining of titanium and its alloys: a review," *Journal of Materials Processing Technology,* vol. 173, pp. 125-135, 2006.

[14] A. Maurotto, A. Roy, V. Babitsky, and V. Silberschmidt, "Recent developments in ultrasonically assisted machining of advanced alloys," in *Proceedings of the 4th*

CIRP International Conference on High Performance Cutting (HPC2010), 2010, pp. 24-26.

[15] R. Muhammad, A. Maurotto, M. Demiral, A. Roy, and V. V. Silberschmidt, "Thermally enhanced ultrasonically assisted machining of Ti alloy," *CIRP Journal of Manufacturing Science and Technology,* vol. 7, pp. 159-167, 2014.

[16] K. Venkatesan, R. Ramanujam, and P. Kuppan, "Analysis of cutting forces and temperature in laser assisted machining of Inconel 718 using Taguchi method," *Procedia Engineering,* vol. 97, pp. 1637-1646, 2014.

[17] M. Farahnakian and M. R. Razfar, "Experimental study on hybrid ultrasonic and plasma aided turning of hardened steel AISI 4140," *Materials and Manufacturing Processes,* vol. 29, pp. 550-556, 2014.

[18] D. Brehl and T. Dow, "Review of vibration-assisted machining," *Precision engineering,* vol. 32, pp. 153-172, 2008.

[19] A. Bhattacharyya, *Metal cutting: theory and practice*: Jamini Kanta Sen of Central Book Publishers, 1984.

[20] G. Boothroyd, "Photographic technique for the determination of metal cutting temperatures," *British Journal of Applied Physics,* vol. 12, pp. 238-242, 1961.

[21] M. A. Davies, Q. Cao, A. Cooks, and R. Ivester, "On the measurement and prediction of temperature fields in machining AISI 1045 steel," *CIRP Annals-Manufacturing Technology,* vol. 52, pp. 77-80, 2003.

[22] C. Leshock and Y. Shin, "Investigation on cutting temperature in turning by a tool-work thermocouple technique," *Journal of manufacturing science and engineering,* vol. 119, pp. 502-508, 1997.

[23] R. Komanduri and W. Reed, "Evaluation of carbide grades and a new cutting geometry for machining titanium alloys," *Wear,* vol. 92, pp. 113-123, 1983.

[24] J. P. Davim, *Surface integrity in machining* vol. 1848828742: Springer, 2010.

[25] G. Ibrahim, C. C. Haron, and J. A. Ghani, "Surface integrity of Ti-6Al-4V ELI when machined using coated carbide tools under dry cutting condition," *International Journal of Mechanical and Materials Engineering,* vol. 4, pp. 191-196, 2009.

[26] C. Che-Haron and A. Jawaid, "The effect of machining on surface integrity of titanium alloy Ti–6% Al–4% V," *Journal of Materials Processing Technology,* vol. 166, pp. 188-192, 2005.

[27] F. Klocke, S. Gierlings, M. Brockmann, and D. Veselovac, "Influence of temperature on surface integrity for typical machining processes in aero engine manufacture," *Procedia Engineering,* vol. 19, pp. 203-208, 2011.

[28] A. Ginting and M. Nouari, "Surface integrity of dry machined titanium alloys," *International Journal of Machine Tools and Manufacture,* vol. 49, pp. 325-332, 2009.

[29] N. Narutaki, A. Murakoshi, S. Motonishi, and H. Takeyama, "Study on machining of titanium alloys," *CIRP Annals-Manufacturing Technology,* vol. 32, pp. 65-69, 1983.

[30] J. Sun and Y. Guo, "A comprehensive experimental study on surface integrity by end milling Ti–6Al–4V," *Journal of Materials Processing Technology,* vol. 209, pp. 4036-4042, 2009.

[31] S. Ramesh, L. Karunamoorthy, and K. Palanikumar, "Surface roughness analysis in machining of titanium alloy," *Materials and Manufacturing Processes,* vol. 23, pp. 174-181, 2008.

[32] S. Pervaiz, A. Rashid, I. Deiab, and M. Nicolescu, "Influence of tool materials on machinability of titanium-and nickel-based alloys: a review," *Materials and Manufacturing Processes,* vol. 29, pp. 219-252, 2014.

[33] J. Hua and R. Shivpuri, "A cobalt diffusion based model for predicting crater wear of carbide tools in machining titanium alloys," *Journal of engineering materials and technology,* vol. 127, pp. 136-144, 2005.

[34] R. C. Skelton, "Turning with an oscillating tool," *International Journal of Machine Tool Design and Research,* vol. 8, pp. 239-259, 1968.

[35] K. Seah, Y. Wong, and L. Lee, "Design of tool holders for ultrasonic machining using FEM," *Journal of Materials Processing Technology,* vol. 37, pp. 801-816, 1993.

[36] M. R. Rani and R. Rudramoorthy, "Computational modeling and experimental studies of the dynamic performance of ultrasonic horn profiles used in plastic welding," *Ultrasonics,* vol. 53, pp. 763-772, 2013.

[37] J. Fluhrer, "DEFORM-3D Version 10.2 user's manual," *Scientific Forming Technologies Corporation,* 2011.

[38] Y. Isik, "Investigating the machinability of tool steels in turning operations," *Materials & design,* vol. 28, pp. 1417-1424, 2007.

[39] E. Ezugwu, "Key improvements in the machining of difficult-to-cut aerospace superalloys," *International Journal of Machine Tools and Manufacture,* vol. 45, pp. 1353-1367, 2005.

[40] E. Ezugwu, J. Bonney, and Y. Yamane, "An overview of the machinability of aeroengine alloys," *Journal of materials processing technology,* vol. 134, pp. 233-253, 2003.

[41] S. Bhaumik, C. Divakar, and A. Singh, "Machining Ti- 6Al- 4V alloy with a wBN-cBN composite tool," *Materials & Design,* vol. 16, pp. 221-226, 1995.

[42] J. Sun and Y. Guo, "Material flow stress and failure in multiscale machining titanium alloy Ti-6Al-4V," *The International Journal of Advanced Manufacturing Technology,* vol. 41, pp. 651-659, 2009.

[43] J. Kahles, M. Field, D. Eylon, and F. Froes, "Machining of titanium alloys," *JOM,* vol. 37, pp. 27-35, 1985.

[44] C. R. Dandekar, Y. C. Shin, and J. Barnes, "Machinability improvement of titanium alloy (Ti–6Al–4V) via LAM and hybrid machining," *International Journal of Machine Tools and Manufacture,* vol. 50, pp. 174-182, 2010.

[45] E. Ezugwu, Z. Wang, and A. Machado, "The machinability of nickel-based alloys: a review," *Journal of Materials Processing Technology,* vol. 86, pp. 1-16, 1999.

[46] C. Che-Haron, "Tool life and surface integrity in turning titanium alloy," *Journal of Materials Processing Technology,* vol. 118, pp. 231-237, 2001.

[47] L. Liang, X. Liu, X.-q. Li, and Y.-Y. Li, "Wear mechanisms of WC–10Ni 3 Al carbide tool in dry turning of Ti6Al4V," *International Journal of Refractory Metals and Hard Materials,* vol. 48, pp. 272-285, 2015.

[48] S. Chauhan and K. Dass, "Optimization of machining parameters in turning of titanium (grade-5) alloy using response surface methodology," *Materials and manufacturing processes,* vol. 27, pp. 531-537, 2012.

[49] S. Ramesh, L. Karunamoorthy, and K. Palanikumar, "Measurement and analysis of surface roughness in turning of aerospace titanium alloy (gr5)," *Measurement,* vol. 45, pp. 1266-1276, 2012.

[50] K. Satyanarayana, A. V. Gopal, and P. B. Babu, "Analysis for optimal decisions on turning Ti–6Al–4V with Taguchi–grey method," *Proceedings of the Institution of Mechanical Engineers, Part C: Journal of Mechanical Engineering Science,* vol. 228, pp. 152-157, 2014.

[51] A. Sharma, M. D. Sharma, and R. Sehgal, "Experimental Study of Machining Characteristics of Titanium Alloy (Ti–6Al–4V)," *Arabian Journal for Science and Engineering*, vol. 38, pp. 3201-3209, 2013.

[52] I. Deiab, S. W. Raza, and S. Pervaiz, "Analysis of lubrication strategies for sustainable machining during turning of titanium Ti-6Al-4V alloy," *Procedia CIRP*, vol. 17, pp. 766-771, 2014.

[53] H. Lin, C. Wang, Y. Yuan, Z. Chen, Q. Wang, and W. Xiong, "Tool wear in Ti-6Al-4V alloy turning under oils on water cooling comparing with cryogenic air mixed with minimal quantity lubrication," *The International Journal of Advanced Manufacturing Technology*, vol. 81, pp. 87-101, 2015.

[54] R. R. Moura, M. B. da Silva, Á. R. Machado, and W. F. Sales, "The effect of application of cutting fluid with solid lubricant in suspension during cutting of Ti-6Al-4V alloy," *Wear*, vol. 332, pp. 762-771, 2015.

[55] M. Dhananchezian and M. P. Kumar, "Cryogenic turning of the Ti–6Al–4V alloy with modified cutting tool inserts," *Cryogenics*, vol. 51, pp. 34-40, 2011.

[56] A. Bordin, S. Bruschi, A. Ghiotti, and P. Bariani, "Analysis of tool wear in cryogenic machining of additive manufactured Ti6Al4V alloy," *Wear*, vol. 328, pp. 89-99, 2015.

[57] A. Nandy, M. Gowrishankar, and S. Paul, "Some studies on high-pressure cooling in turning of Ti–6Al–4V," *International Journal of Machine Tools and Manufacture*, vol. 49, pp. 182-198, 2009.

[58] S. Palanisamy, S. D. McDonald, and M. S. Dargusch, "Effects of coolant pressure on chip formation while turning Ti6Al4V alloy," *International Journal of Machine Tools and Manufacture*, vol. 49, pp. 739-743, 2009.

[59] J. Xie, M. Luo, K. Wu, L. Yang, and D. Li, "Experimental study on cutting temperature and cutting force in dry turning of titanium alloy using a non-coated micro-grooved tool," *International Journal of Machine Tools and Manufacture*, vol. 73, pp. 25-36, 2013.

[60] J. Ma, N. H. Duong, and S. Lei, "3D numerical investigation of the performance of microgroove textured cutting tool in dry machining of Ti-6Al-4V," *The International Journal of Advanced Manufacturing Technology*, vol. 79, pp. 1313-1323, 2015.

[61] A. Daymi, M. Boujelbene, S. B. Salem, B. H. Sassi, and S. Torbaty, "Effect of the cutting speed on the chip morphology and the cutting forces," *Archives of*

Computational Materials Science and Surface Engineering, vol. 1, pp. 77-83, 2009.

[62] M. Cotterell and G. Byrne, "Characterisation of chip formation during orthogonal cutting of titanium alloy Ti–6Al–4V," *CIRP Journal of Manufacturing Science and Technology,* vol. 1, pp. 81-85, 2008.

[63] M. V. Ramana, G. K. M. Rao, and D. H. Rao, "Chip morphology in turning of Ti-6Al-4V alloy under different machining conditions," *Journal of Production Engineering,* vol. 17, pp. 27-32, 2014.

[64] Q. An, Y. Fu, and J. Xu, "Experimental study on turning of TC9 titanium alloy with cold water mist jet cooling," *International Journal of Machine Tools and Manufacture,* vol. 51, pp. 549-555, 2011.

[65] D. Ensminger and L. J. Bond, *Ultrasonics: fundamentals, technologies, and applications*: CRC press, 2011.

[66] J. Kumabe, "Vibratory cutting," *Dzikke Sjuppan, Tokyo,* 1979.

[67] J. Kumabe and M. Hachisuka, "Super-precision cylindrical machining," *Precision engineering,* vol. 6, pp. 67-72, 1984.

[68] J. Kumabe, K. Fuchizawa, T. Soutome, and Y. Nishimoto, "Ultrasonic superposition vibration cutting of ceramics," *Precision Engineering,* vol. 11, pp. 71-77, 1989.

[69] J. R. Frederick, "Ultrasonic engineering," 1965.

[70] M. Zhou, X. Wang, B. Ngoi, and J. Gan, "Brittle–ductile transition in the diamond cutting of glasses with the aid of ultrasonic vibration," *Journal of Materials Processing Technology,* vol. 121, pp. 243-251, 2002.

[71] V. Astashev and V. Babitsky, "Ultrasonic cutting as a nonlinear (vibro-impact) process," *Ultrasonics,* vol. 36, pp. 89-96, 1998.

[72] J.-D. Kim and E.-S. Lee, "A study of the ultrasonic-vibration cutting of carbon-fiber reinforced plastics," *Journal of materials processing technology,* vol. 43, pp. 259-277, 1994.

[73] A. Mitrofanov, V. Babitsky, and V. V. Silberschmidt, "Finite element simulations of ultrasonically assisted turning," *Computational Materials Science,* vol. 28, pp. 645-653, 2003.

[74] N. Ahmed, A. Mitrofanov, V. Babitsky, and V. Silberschmidt, "Analysis of forces in ultrasonically assisted turning," *Journal of Sound and Vibration,* vol. 308, pp. 845-854, 2007.

[75] M. Khajehzadeh, M. Akhlaghi, and M. Razfar, "Finite element simulation and experimental investigation of tool temperature during ultrasonically assisted turning of aerospace aluminum using multicoated carbide inserts," *The International Journal of Advanced Manufacturing Technology,* vol. 75, pp. 1163-1175, 2014.

[76] V. Babitsky, A. Kalashnikov, A. Meadows, and A. Wijesundara, "Ultrasonically assisted turning of aviation materials," *Journal of materials processing technology,* vol. 132, pp. 157-167, 2003.

[77] A. Mitrofanov, V. Babitsky, and V. Silberschmidt, "Finite element analysis of ultrasonically assisted turning of Inconel 718," *Journal of materials processing technology,* vol. 153, pp. 233-239, 2004.

[78] A. Mitrofanov, V. Babitsky, and V. Silberschmidt, "Thermomechanical finite element simulations of ultrasonically assisted turning," *Computational materials science,* vol. 32, pp. 463-471, 2005.

[79] A. Mitrofanov, N. Ahmed, V. Babitsky, and V. Silberschmidt, "Effect of lubrication and cutting parameters on ultrasonically assisted turning of Inconel 718," *Journal of materials processing technology,* vol. 162, pp. 649-654, 2005.

[80] N. Ahmed, A. Mitrofanov, V. Babitsky, and V. Silberschmidt, "Analysis of material response to ultrasonic vibration loading in turning Inconel 718," *Materials Science and Engineering: A,* vol. 424, pp. 318-325, 2006.

[81] S. Amini, H. Soleimanimehr, M. Nategh, A. Abudollah, and M. Sadeghi, "FEM analysis of ultrasonic-vibration-assisted turning and the vibratory tool," *Journal of materials processing technology,* vol. 201, pp. 43-47, 2008.

[82] C. Nath, M. Rahman, and S. Andrew, "A study on ultrasonic vibration cutting of low alloy steel," *Journal of Materials Processing Technology,* vol. 192, pp. 159-165, 2007.

[83] C. Nath and M. Rahman, "Effect of machining parameters in ultrasonic vibration cutting," *International Journal of Machine Tools and Manufacture,* vol. 48, pp. 965-974, 2008.

[84] C. Nath, M. Rahman, and K. S. Neo, "Modeling of the effect of machining parameters on maximum thickness of cut in ultrasonic elliptical vibration cutting," *Journal of manufacturing science and engineering,* vol. 133, pp. 0110071-0110078, 2011.

[85] C. Nath, M. Rahman, and K. S. Neo, "A study on the effect of tool nose radius in ultrasonic elliptical vibration cutting of tungsten carbide," *Journal of Materials Processing Technology*, vol. 209, pp. 5830-5836, 2009.

[86] S. Koshimizu, "Ultrasonic vibration-assisted cutting of titanium alloy," in *Key Engineering Materials*, 2009, pp. 277-282.

[87] R. Muhammad, N. Ahmed, M. Demiral, A. Roy, and V. V. Silberschmidt, "Computational study of ultrasonically-assisted turning of Ti alloys," in *Advanced Materials Research*, 2011, pp. 30-36.

[88] R. Muhammad, N. Ahmed, A. Roy, and V. V. Silberschmidt, "Numerical modelling of vibration-assisted turning of Ti-15333," *Procedia CIRP*, vol. 1, pp. 347-352, 2012.

[89] R. Muhammad, A. Maurotto, A. Roy, and V. V. Silberschmidt, "Hot ultrasonically assisted turning of β-Ti alloy," *Procedia CIRP*, vol. 1, pp. 336-341, 2012.

[90] R. Muhammad, M. S. Hussain, A. Maurotto, C. Siemers, A. Roy, and V. V. Silberschmidt, "Analysis of a free machining α+ β titanium alloy using conventional and ultrasonically assisted turning," *Journal of Materials Processing Technology*, vol. 214, pp. 906-915, 2014.

[91] R. Muhammad, A. Roy, and V. V. Silberschmidt, "Finite element modelling of conventional and hybrid oblique turning processes of titanium alloy," *Procedia CIRP*, vol. 8, pp. 510-515, 2013.

[92] S. Patil, S. Joshi, A. Tewari, and S. S. Joshi, "Modelling and simulation of effect of ultrasonic vibrations on machining of Ti6Al4V," *Ultrasonics*, vol. 54, pp. 694-705, 2014.

[93] M. Nategh, H. Razavi, and A. Abdullah, "Analytical modeling and experimental investigation of ultrasonic-vibration assisted oblique turning, part I: kinematics analysis," *International Journal of Mechanical Sciences*, vol. 63, pp. 1-11, 2012.

[94] H. Jamshidi and M. Nategh, "Theoretical and experimental investigation of the frictional behavior of the tool–chip interface in ultrasonic-vibration assisted turning," *International Journal of Machine Tools and Manufacture*, vol. 65, pp. 1-7, 2013.

[95] G. Dong, H. Zhang, M. Zhou, and Y. Zhang, "Experimental investigation on ultrasonic vibration-assisted turning of SiCp/Al composites," *Materials and Manufacturing Processes*, vol. 28, pp. 999-1002, 2013.

[96] M. Khajehzadeh, M. R. Razfar, and M. Akhlaghi, "Experimental Investigation of Tool Temperature During Ultrasonically Assisted Turning of Aerospace Aluminum," *Materials and Manufacturing Processes*, vol. 29, pp. 1453-1460, 2014.

[97] P. Zou, Y. Xu, Y. He, M. Chen, and H. Wu, "Experimental Investigation of Ultrasonic Vibration Assisted Turning of 304 Austenitic Stainless Steel," *Shock and Vibration,* vol. 2015, pp. 1-19, 2015.

[98] M. Xiao, S. Karube, T. Soutome, and K. Sato, "Analysis of chatter suppression in vibration cutting," *International Journal of Machine Tools and Manufacture*, vol. 42, pp. 1677-1685, 2002.

[99] L.-J. Wang and J. Zhao, "Influence on surface roughness in turning with ultrasonic vibration tool," *International journal of machine tools and manufacture,* vol. 27, pp. 181-190, 1987.

[100] V. Babitsky, A. Mitrofanov, and V. Silberschmidt, "Ultrasonically assisted turning of aviation materials: simulations and experimental study," *Ultrasonics,* vol. 42, pp. 81-86, 2004.

[101] D. Ensminger and F. B. Stulen, *Ultrasonics: data, equations and their practical uses*: CRC press, 2008.

[102] M. Nad', "Ultrasonic horn design for ultrasonic machining technologies," *Applied and Computational Mechanics*, vol. 4, pp. 79-88, 2010.

[103] A. S. Nanu, N. I. Marinescu, and D. Ghiculescu, "Study on ultrasonic stepped horn geometry design and FEM simulation," *Nonconventional Technologies Review*, pp. 25-30, 2011.

[104] S. Amin, M. Ahmed, and H. Youssef, "Computer-aided design of acoustic horns for ultrasonic machining using finite-element analysis," *Journal of Materials Processing Technology*, vol. 55, pp. 254-260, 1995.

[105] V. Yadava and A. Deoghare, "Design of horn for rotary ultrasonic machining using the finite element method," *The International Journal of Advanced Manufacturing Technology*, vol. 39, pp. 9-20, 2008.

[106] A. Cardoni, A. MacBeath, and M. Lucas, "Methods for reducing cutting temperature in ultrasonic cutting of bone," *Ultrasonics*, vol. 44, pp. e37-e42, 2006.

[107] K.-M. Shu, W.-H. Hsieh, and H.-S. Yen, "On the design and analysis of acoustic horns for ultrasonic welding," *Transactions of the Canadian Society for Mechanical Engineering*, vol. 37, pp. 905-916, 2013.

[108] K.-M. Shu and J.-W. Chen, "The Design of Acoustic Horns for Ultrasonic Aided Tube Double Side Flange Making," *World Academy of Science, Engineering and Technology, International Journal of Mechanical, Aerospace, Industrial, Mechatronic and Manufacturing Engineering,* vol. 9, pp. 838-841, 2015.

[109] H.-D. T. Nguyen and D.-A. Wang, "Design of an Ultrasonic Steel Horn with a Bézier Profile," *International Conference on Green Technology and Sustainable Development,* vol. 9, pp. 475-485, 2013.

[110] J. Mackerle, "Finite-element analysis and simulation of machining: a bibliography (1976–1996)," *Journal of Materials Processing Technology,* vol. 86, pp. 17-44, 1999.

[111] J. Mackerle, "Finite element analysis and simulation of machining: an addendum: a bibliography (1996–2002)," *International Journal of Machine Tools and Manufacture,* vol. 43, pp. 103-114, 2003.

[112] P. Arrazola, T. Özel, D. Umbrello, M. Davies, and I. Jawahir, "Recent advances in modelling of metal machining processes," *CIRP Annals-Manufacturing Technology,* vol. 62, pp. 695-718, 2013.

[113] D. Umbrello, "Finite element simulation of conventional and high speed machining of Ti6Al4V alloy," *Journal of materials processing technology,* vol. 196, pp. 79-87, 2008.

[114] R. Li and A. J. Shih, "Finite element modeling of 3D turning of titanium," in *ASME 2004 International Mechanical Engineering Congress and Exposition*, 2004, pp. 825-833.

[115] H. Bil, S. E. Kılıç, and A. E. Tekkaya, "A comparison of orthogonal cutting data from experiments with three different finite element models," *International Journal of Machine Tools and Manufacture,* vol. 44, pp. 933-944, 2004.

[116] V. Schulze and F. Zanger, "Numerical Analysis of the Influence of Johnson-Cook-Material Parameters on the Surface Integrity of Ti-6Al-4V," *Procedia Engineering,* vol. 19, pp. 306-311, 2011.

[117] M. H. Ali, B. A. Khidhir, B. Mohamed, and A. Oshkour, "Prediction of High Cutting Speed Parameters for Ti-6Al-4V by Using Finite Element Modeling," *International Journal of Modeling and Optimization,* vol. 2, pp. 31-35, 2012.

[118] Y. Karpat, "Temperature dependent flow softening of titanium alloy Ti6Al4V: An investigation using finite element simulation of machining," *Journal of Materials Processing Technology,* vol. 211, pp. 737-749, 2011.

[119] M. Calamaz, D. Coupard, and F. Girot, "A new material model for 2D numerical simulation of serrated chip formation when machining titanium alloy Ti–6Al–4V," *International Journal of Machine Tools and Manufacture*, vol. 48, pp. 275-288, 2008.

[120] W.-S. Lee and C.-F. Lin, "Plastic deformation and fracture behaviour of Ti–6Al–4V alloy loaded with high strain rate under various temperatures," *Materials Science and Engineering: A*, vol. 241, pp. 48-59, 1998.

[121] R. Shivpuri, J. Hua, P. Mittal, A. Srivastava, and G. Lahoti, "Microstructure-mechanics interactions in modeling chip segmentation during titanium machining," *CIRP Annals-Manufacturing Technology*, vol. 51, pp. 71-74, 2002.

[122] T. Özel and E. Zeren, "Determination of work material flow stress and friction for FEA of machining using orthogonal cutting tests," *Journal of Materials Processing Technology*, vol. 153, pp. 1019-1025, 2004.

[123] H. W. Meyer and D. S. Kleponis, "Modeling the high strain rate behavior of titanium undergoing ballistic impact and penetration," *International Journal of Impact Engineering*, vol. 26, pp. 509-521, 2001.

[124] L. Filice, D. Umbrello, F. Micari, and L. Settineri, "On the finite element simulation of thermal phenomena in machining processes," in *Advanced Methods in Material Forming*, ed: Springer, 2007, pp. 263-278.

[125] L. Filice, D. Umbrello, S. Beccari, and F. Micari, "On the FE codes capability for tool temperature calculation in machining processes," *Journal of Materials Processing Technology*, vol. 174, pp. 286-292, 2006.

[126] R. Muhammad, A. Maurotto, A. Roy, and V. Silberschmidt, "Ultrasonically assisted turning of Ti-6Al-2Sn-4Zr-6Mo," in *Journal of Physics: Conference Series*, 2012, pp. 12-16.

[127] M. Naď, "Ultrasonic horn design for ultrasonic machining technologies," *Applied and Computational Mechanics*, vol. 4, 2010.

[128] "Ansys Mechanical User's, Release 15," *Ansys Inc., Canonsburg*, pp. 1531-1832, 2015.

[129] A. I. H. Committee, "Metals handbook: vol. 1 Properties and selection: irons, steels, and high-performance alloys," *Ohio: ASM International*, 1990.

[130] H. Mercier, W. J. Ammann, F. Deischl, J. Eisenmann, I. Floegl, G. H. Hirsch, *et al.*, *Vibration problems in structures: practical guidelines*: Birkhäuser, 2012.

[131] H. O. Pierson, *Handbook of Refractory Carbides & Nitrides: Properties, Characteristics, Processing and Apps*: William Andrew, 1996.

[132] P. D. Harvey, *Engineering properties of steel*: Asm Intl, 1982.

[133] M. Nayak and R. Sehgal, "Effect of Tool Material Properties and Cutting Conditions on Machinability of AISI D6 Steel During Hard Turning," *Arabian Journal for Science and Engineering,* vol. 40, pp. 1151-1164, 2015.

[134] S. Sheth and P. George, "Experimental investigation, prediction and optimization of cylindricity and perpendicularity during drilling of WCB material using grey relational analysis," *Precision Engineering,* vol. 45, pp. 33-43, 2016.

[135] L. Lehman and J. Gould, "A design-of-experiments evaluation of resistance spot welding manufacturability—part 3: optimization and process robustness studies," *IBEC 96 Proceedings, Advanced Technologies and Processes,* 1996.

[136] G. Bartarya and S. Choudhury, "Effect of cutting parameters on cutting force and surface roughness during finish hard turning AISI52100 grade steel," *Procedia CIRP,* vol. 1, pp. 651-656, 2012.

[137] L. Filice, F. Micari, S. Rizzuti, and D. Umbrello, "A critical analysis on the friction modelling in orthogonal machining," *International Journal of Machine Tools and Manufacture,* vol. 47, pp. 709-714, 2007.

[138] D. Umbrello, L. Filice, S. Rizzuti, F. Micari, and L. Settineri, "On the effectiveness of finite element simulation of orthogonal cutting with particular reference to temperature prediction," *Journal of Materials Processing Technology,* vol. 189, pp. 284-291, 2007.

[139] J. Hua and R. Shivpuri, "Prediction of chip morphology and segmentation during the machining of titanium alloys," *Journal of Materials Processing Technology,* vol. 150, pp. 124-133, 2004.

[140] V. V. Silberschmidt, S. M. Mahdy, M. A. Gouda, A. Naseer, A. Maurotto, and A. Roy, "Surface-roughness improvement in ultrasonically assisted turning," *Procedia CIRP,* vol. 13, pp. 49-54, 2014.

[141] J. Colafemina, R. Jasinevicius, and J. Duduch, "Surface integrity of ultra-precision diamond turned Ti (commercially pure) and Ti alloy (Ti-6Al-4V)," *Proceedings of the Institution of Mechanical Engineers, Part B: Journal of Engineering Manufacture,* vol. 221, pp. 999-1006, 2007.

Dissemination

Conferences [1]

1. R Kandi and S K Sahoo, "Design and Modeling of a Flexible Acoustic Horn for Ultrasonic Vibration Assisted Turning," *Proceedings of International Conference on Advances in Dynamics, Vibration and Control, ICADVC- 2016*, National Institute of Technology, Durgapur, pp. 197-201, 2016
2. R Kandi and S K Sahoo, "Experimental investigation on machinability of Titanium alloy, Ti-6Al-4V during ultrasonic vibration assisted turning" *Proceedings of All India Manufacturing, Technology, Design and Research Conference. (AIMTDR-2016), 16th -18th December 2016*

[1] Articles already published, in press, or formally accepted for publication
[2] Articles under review, communicated, or to be communicated